Journal of Neuroinflammation

RESEARCH

Open Access

IRF3 regulates neuroinflammatory responses and the expression of genes associated with Alzheimer's disease

Radhika Joshi[1], Veronika Brezani[1], Gabrielle M. Mey[2,3], Sergi Guixé-Muntet[4], Marti Ortega-Ribera[1], Yuan Zhuang[1], Adam Zivny[1], Sebastian Werneburg[2,3], Jordi Gracia-Sancho[4,5] and Gyongyi Szabo[1*]

Abstract

The pathological role of interferon signaling is emerging in neuroinflammatory disorders, yet, the specific role of Interferon Regulatory Factor 3 (IRF3) in neuroinflammation remains poorly understood. Here, we show that global IRF3 deficiency delays TLR4-mediated signaling in microglia and attenuates the hallmark features of LPS-induced inflammation such as cytokine release, microglial reactivity, astrocyte activation, myeloid cell infiltration, and inflammasome activation. Moreover, expression of a constitutively active IRF3 (S388D/S390D: IRF3-2D) in microglia induces a transcriptional program reminiscent of the Activated Response Microglia and the expression of genes associated with Alzheimer's disease, notably apolipoprotein-e. Using bulk-RNAseq of IRF3-2D brain myeloid cells, we identified Z-DNA binding protein-1 (ZBP1) as a target of IRF3 that is relevant across various neuroinflammatory disorders. Lastly, we show IRF3 phosphorylation and IRF3-dependent ZBP1 induction in response to Aβ in primary microglia cultures. Together, our results identify IRF3 as an important regulator of LPS and Aβ -mediated neuroinflammatory responses and highlight IRF3 as a central regulator of disease-specific gene activation in different neuroinflammatory diseases.

Keywords Amyloid beta, APOE, IRF3, Type 1 interferon, ARM, IRM, Neuroinflammation, Alzheimer's disease, DAM, ZBP1

Introduction

Type I interferon (IFN-I) signaling is a critical adaptive immune response best known to combat viral infections [1, 2]. The role of IFN-I signaling in the regulation of innate immunity and sterile inflammatory conditions is increasingly recognized. The pathological role of interferon signaling has been reported in a variety of neurological disorders including Alzheimer's disease (AD), Down syndrome, traumatic brain injury (TBI), and stroke [3–8]. Interferon signaling is also associated with behavioral changes such as cognitive decline, anxiety, depression, and susceptibility to stress [9–11]. Interferonopathies are another class of neuropathological disorders specifically classified as such based on their excessive activation of interferon signaling [12]. Relevant to the role of IFN-I, single nucleotide polymorphisms in interferon-stimulated genes (ISGs) have been associated with AD [13].

Single-cell RNA sequencing techniques have discovered interferon-responsive microglia (IRMs with antiviral

*Correspondence:
Gyongyi Szabo
gszabo1@bidmc.harvard.edu
[1] Department of Medicine, Beth Israel Deaconess Medical Center and Harvard Medical School, Boston, USA
[2] Department of Opthalmology and Visual Sciences, Kellogg Eye Center Michigan Neuroscience Institute, University of Michigan, Ann Arbor, USA
[3] Michigan Neuroscience Institute, University of Michigan, Ann Arbor, MI, USA
[4] Liver Vascular Biology, IDIBAPS Biomedical Research Institute-CIBEREHD, Barcelona, Spain
[5] Department of Visceral Surgery and Medicine, Inselspital, Bern University Hospital, University of Bern, Bern, Switzerland

immune response) in diseases such as AD, multiple sclerosis (MS) and during natural aging [14–16]. IFN-responsive astrocytes and oligodendrocytes have also been described in AD models and aging [17, 18]. However, a comprehensive understanding of the underlying molecular mechanisms and function of these cell types is still under investigation.

Interferon signaling is regulated via 9 transcription factors called interferon response factors IRF1-9 [19]. Among these, IRF3 is at the crossroads of adaptive and innate immune responses. IRF3 activation is triggered downstream of TLR3, RIG-I, and MDA-5 in response to dsRNA, typically observed during viral infections [19]. IRF3 is also activated downstream of TLR4 in a MyD88 independent fashion involving the TRIF adapter molecule [20, 21]. Following TLR3/4 activation, IRF3 undergoes phosphorylation and dimerization leading to nuclear entry that drives the expression of ISGs [19, 21]. While IRF3-mediated signaling has been well-studied in various models of peripheral inflammation [20, 22–25], in-depth studies directly investigating the role of IRF3 in neuroinflammatory conditions are lacking.

In this study, we examined the direct consequences of IRF3 perturbations on neuroinflammation and microglia. We used the commonly used model of neuroinflammation induced by lipopolysaccharides (LPS), to mimic TLR4 activation. We observed that IRF3 plays a critical role in various features of LPS-mediated proinflammatory changes such as sickness behavior, cytokine production, myeloid cell infiltration and inflammasome activation. Furthermore, we showed that the mere expression of a constitutively active form of IRF3 (IRF3-2D) is sufficient to trigger a proinflammatory phenotype in microglia reminiscent of the IRMs. Importantly, IRF3 activation leads to the expression of genes associated with AD, most notably, apolipoprotein-e (*Apoe)*. In addition, we compared the transcriptome of brain myeloid cells from the IRF3-2D mouse model to that of other neuroinflammatory conditions. We identified *Zbp1* as one of the common proinflammatory signatures in microglia across different neurological disorders and we show that IRF3 directly regulates ZBP1. Lastly, we showed that Aβ induces IRF3 phosphorylation and drives the expression of ZBP1 in IRF3 dependent fashion in microglia. Taken together, we demonstrate that IRF3 plays an important role in proinflammatory responses induced by LPS and Aβ. Furthermore, selective activation of IRF3 induces features of IRM and certain AD-associated genes.

Results

IRF3KO mice show attenuated sickness behavior and reduced proinflammatory and IFN responses after an acute LPS challenge

To determine the relative contribution of the IRF3-induced signaling cascade on the proinflammatory effects of LPS, we first administered LPS (1 mg/kg) to wild type (WT) and IRF3KO (whole body knockout) mice. Mice were euthanized 6 h later. We analyzed LPS-induced sickness behavior (Fig. 1A) in the open field test and observed that WT mice showed reduced locomotion and velocity ~ 5 h after LPS administration compared to the vehicle group. This reduction in activity was significantly attenuated in the IRF3KO-LPS treated group (Fig. 1B). Since sickness behavior is correlated to the peripheral and central nervous system (CNS) release of cytokines such as IL1β, TNFα, IL6 [26, 27], we assessed the levels of different cytokines and chemokines in cortical lysates and serum. We found a significant upregulation in IL1β, IL6, IL1α, MCP1, and CXCL1 levels in the cortices of mice treated with LPS in the WT group (Fig. 1C). However, cytokine (IL1β, IL1α, IL6) and chemokine (MCP1, CXCL1) induction by LPS was absent or significantly attenuated in cortices of IRF3KO mice (Fig. 1C). In the serum we observed significant upregulation of IL1β, IL6 and TNFα in the WT-LPS sera, but the induction of these cytokines was significantly attenuated or absent in the IRF3KO-LPS sera (Fig. 1D). Together, we observed that IRF3KO mice show reduced systemic pro-inflammatory response to LPS.

IRF3 deletion delays TLR4 signaling and dampens cytokine secretion in primary microglia cultures

Next we evaluated the specific role of IRF3 in primary microglia cultures. The rationale here was two fold. First, microglia are the key mediators of proinflammatory responses in the CNS. Second, reduced peripheral inflammation in the IRF3KO-LPS mice (Fig. 1D) complicates the interpretation of cell-type specific IRF3

(See figure on next page.)

Fig. 1 IRF3 deletion attenuates the proinflammatory effects of acute LPS challenge. **A** Schematic of the acute LPS challenge model. Sickness behavior was recorded in the open field arena ~ 5 h after i.p. (intraperitoneal) LPS administration and tissue was collected after 6 h. **B** Quantification of distance traveled and velocity of movement in open field arena shows that IRF3KO mice display attenuated sickness behavior compared to the WT. N = 11–13 for each group. **C** & **D** Quantification of ELISA from cortical lysates (1C) and sera (1D) show that proinflammatory cytokines are significantly upregulated in WT mice on LPS challenge but remain significantly reduced in the IRF3KO cortices and serum compared to the WT. N = 11–13 for each group. Two-way ANOVA with Tukey's multiple comparisons. *p < 0.05, **p < 0.01, ***p < 0.001, ****p < 0.0001

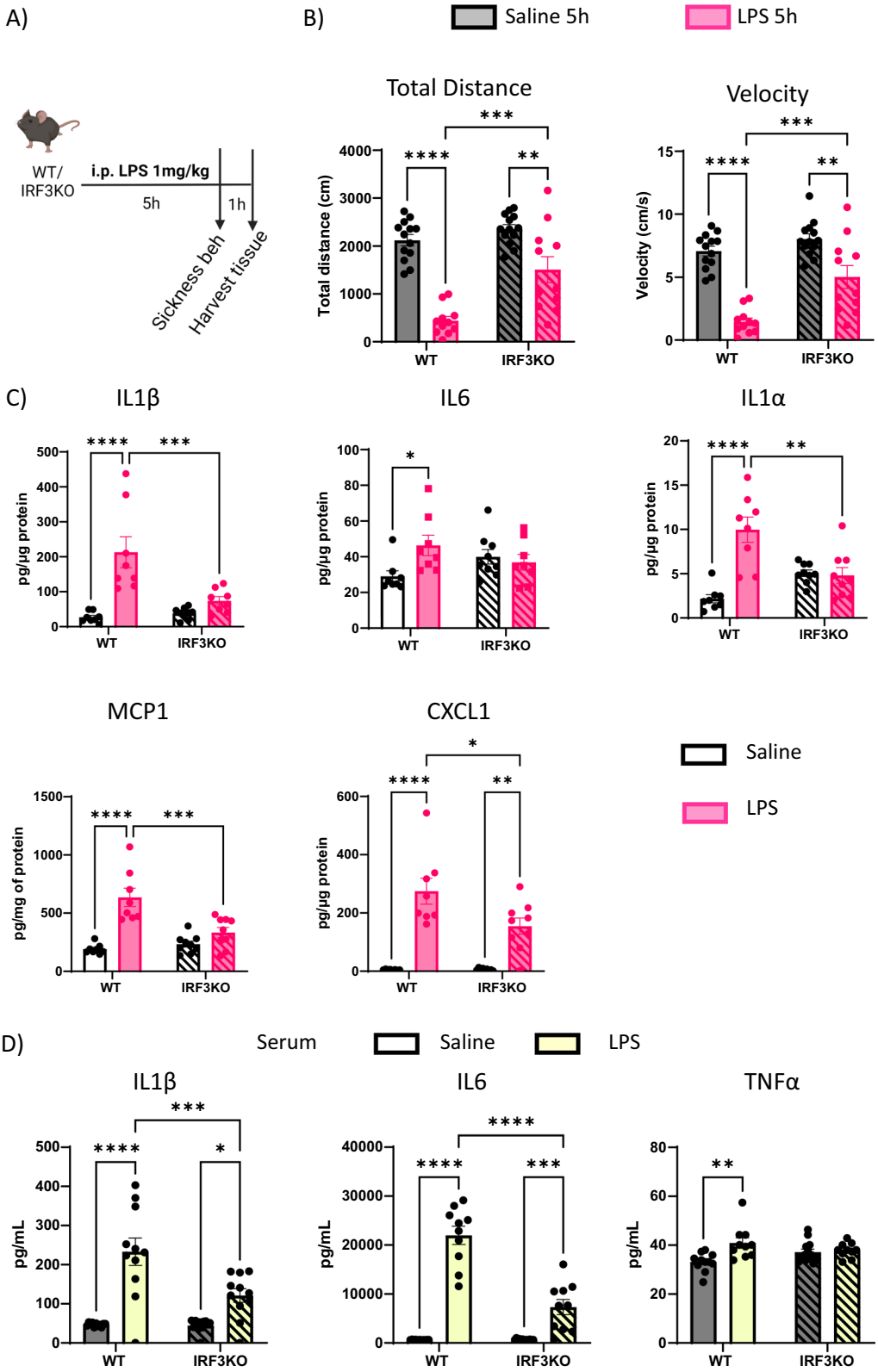

Fig. 1 (See legend on previous page.)

signaling. Hence, we assessed IRF3 signaling in primary microglia cultures after LPS (20 ng/mL) stimulation at 30 min and 120 min time points. First, we established that LPS induces IRF3 phosphorylation (Fig. 2A, B) and nuclear translocation (Supplementary Fig. 1) in microglia. TLR4 activation leads to MyD88 dependent and independent signaling cascade that can feedback onto each other [21, 28, 29]. To this end, we generated primary microglia cultures from WT and IRF3KO mice and assessed the phosphorylation of the key signaling cascades downstream of TLR4 activation: NF-κB (p65), p38, and ERK1/2 (Fig. 2C).

As expected, 30 min after in vitro LPS addition, there was significant phosphorylation of the secondary signaling molecules- NF-κB (p65), p38, and ERK1/2 in the WT and IRF3KO microglia, as shown by the mean fold change > 1 (over vehicle-treated samples) for phospho/total protein (Fig. 2C, D). However, microglia isolated from IRF3KO mice showed strikingly lower phosphorylation levels of all the three signaling molecules at 30 min. Notably, the phosphorylation of NF-κB continued to be significantly lower in the IRF3KO cultures for up to 120 min after LPS stimulation whereas p-p38 and pERK1/2 were comparable to WT microglia (Fig. 2D, E).

In addition, we observed significantly attenuated release of cytokines in the supernatant of LPS-treated cultures of IRF3KO microglia (IFNβ, TNFα, IL6, and IL1α) when compared to the WT microglia (Fig. 2F).

Together, our in vitro data shows an important regulatory role of IRF3 in LPS-mediated TLR4 signaling and cytokine production in microglia.

To assess the cell-specific responses in vivo, we tested the expression of proinflammatory transcripts in flow-sorted microglia ($CD11b^{+}$,$CD45^{intermediate}$) (Fig. 3A). IRF3 is critical for interferon responses downstream of TLR4, thus we first assessed signatures of interferon signaling followed by other proinflammatory mediators. LPS stimulation induced signatures of interferon signaling (*Ifit1, Isg15, Gbp2*) in WT mice, but these ISGs expression after LPS treatment was abrogated in IRF3KO mice (Fig. 3B–D). Similarly, proinflammatory transcripts of *Cox2* and *H2-D1* were significantly increased in microglia of the WT-LPS but not in the IRF3KO-LPS group (Fig. 3E, F). Interestingly, IRF3KO mice showed more sensitivity to LPS-induced *C3* transcripts compared to the WT (Fig. 3G) and downregulation of the homeostatic marker *P2ry12* was comparable between WT and IRF3KO after acute LPS injection (Fig. 3H). These data collectively suggested that IRF3 partially contributes to the proinflammatory effects of LPS in microglia.

IRF3 is expressed by all the major cell types in the brain including astrocytes [30]. Thus, we also tested the proinflammatory state of flow-sorted $CD11b^{-}ACSA\text{-}2^{+}$ astrocytes in IRF3KO mice (Fig. 3A). We observed that LPS-induced upregulation of interferon signaling (*Ifit, Gbp2, and Igtp*) (Fig. 3 I–K) and *Gfap* (Fig. 3L) were significantly lower in the IRF3KO-LPS mice compared to the WT-LPS group, suggesting that IRF3 is important for LPS-mediated astrocyte activation (Fig. 3I–L).

IRF3KO mice show reduced myeloid cell infiltration and inflammasome activation in the brain after repeated LPS challenges

IFN-I signaling is implicated in myeloid cell infiltration [31]. However, the contribution of IRF3 specifically in the context of myeloid cell infiltration in the CNS is unexplored.

No monocyte infiltration was detected in response to 6 h of single LPS injection in vivo in our model (Supplementary Fig. 2A). Also, in chronic neuroinflammatory conditions TLR activation occurs constitutively or repeatedly. Thus, we next tested IRF3 activation and its downstream effects in a repeated LPS challenge paradigm. Here, mice were treated with a 1 mg/kg dose of LPS daily for 4 days and euthanized 6 h after the last LPS dose (Fig. 4A).

(See figure on next page.)

Fig. 2 IRF3 deficient primary microglia cultures show delayed downstream signaling and attenuated cytokine production on LPS challenge. **A** and **C** Representative images of western blots from primary microglia cultures treated with LPS. **B** Quantification of the westerns show significant IRF3 phosphorylation in the WT cells, following LPS stimulation. N = 6 for each group. Mann–Whitney test, $^{**}p < 0.01$. **D** Quantification shows that 30 min after LPS stimulation, there is an increase in phosphorylation of NF-κB, p38, and ERK1/2 as indicated by the fold change > 1 over the 0-time point in WT and IRF3KO cultures. However, IRF3KO microglia cultures show significant reduction in the levels of phosphorylation compared to that of WT. N = 7,8 for each group. Mann–Whitney test, $^{*}p < 0.05$, $^{**}p < 0.01$, $^{***}p < 0.001$, $^{****}p < 0.0001$. **E** Quantification shows that 120 min after LPS stimulation, there is an increase in phosphorylation of NF-κB, p38, and ERK1/2 as indicated by the fold change > 1 over the 0-time point for both genotypes. However, IRF3KO microglia cultures only show a significant reduction in the levels of phosphorylation of NF-κB, while those of p38 and ERK1/2 are indistinguishable from that of the WT. N = 7,8 for each group. Mann–Whitney test or unpaired t-test as appropriate. $^{*}p < 0.05$, $^{**}p < 0.01$, $^{***}p < 0.001$, $^{****}p < 0.0001$. **F** Quantification of ELISA from cell culture supernatants shows that proinflammatory cytokines (IFNβ, TNFα, IL6, ILβ, IL1α) are significantly upregulated in WT microglia on LPS challenge. IRF3KO cultures show either no release or significantly reduced release of cytokines on LPS challenge. N = 4–7 for each group. Two-way ANOVA with Tukey's multiple comparisons. $^{*}p < 0.05$, $^{**}p < 0.01$, $^{***}p < 0.001$, $^{****}p < 0.0001$

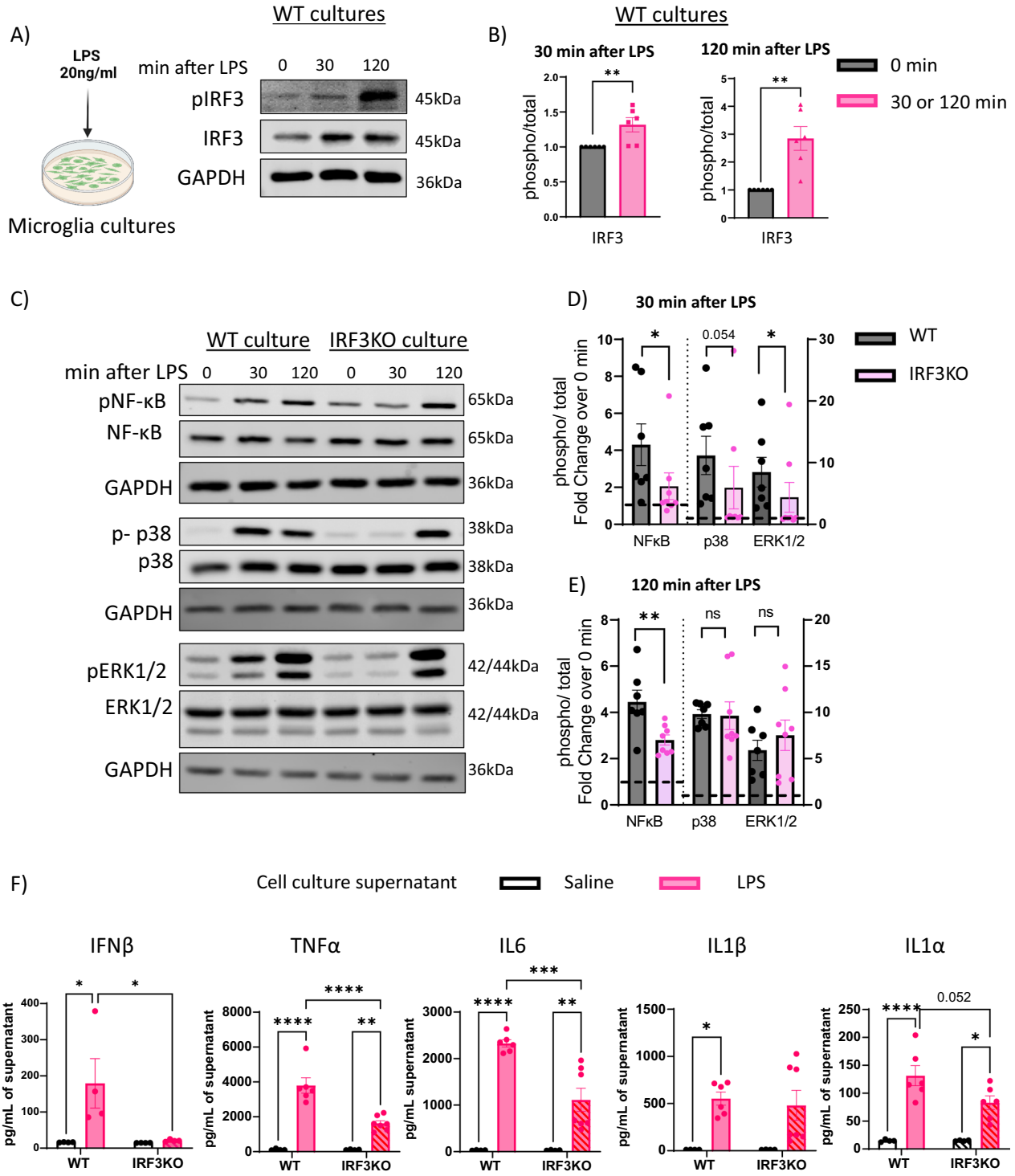

Fig. 2 (See legend on previous page.)

In the WT-LPS group, we observed a distinct population of CD11b^{+},CD45^{high} cells, in addition to the resident microglia population defined as CD11b^{+},CD45^{intermediate}, suggesting infiltration of peripheral myeloid cells upon repeated LPS challenges (Fig. 4B,C,D). In contrast to WT, IRF3KO mice showed significantly reduced infiltration of myeloid cells (Fig. 4B,C,D). We also determined that this myeloid cell

infiltration took place in the absence of damage to the blood–brain barriers in our model of 4-day LPS challenge as indicated by no changes in the expression of blood brain barrier markers, (Claudin-1 and Occludin) (Supplementary Fig. 3A–C) or extravasation of FITC-Albumin in brain parenchyma (Supplementary Fig. 3D–F).

Moreover, the microglia population of IRF3KO-LPS group showed significantly lower CD11b expression (gated on the $CD11b^{+}$,$CD45^{intermediate}$ microglia population) compared to the WT-LPS group (Fig. 4E,F), further suggesting an overall less proinflammatory effect of IRF3 deletion on microglia.

Because in the acute model, we also observed proinflammatory transcripts in astrocytes, we tested whether astrocyte reactivity was also affected after 4 days of repeated LPS challenge in IRF3 deficient mice. Assessment of GFAP levels in the cortex by western blots revealed a modest, yet significant, attenuation of GFAP levels in the IRF3KO-LPS mice compared to the WT-LPS mice (Fig. 4G, I).

Because, we found attenuated IL1β induction in the cortex after acute LPS challenge in IRF3KO mice (Fig. 1C) we were curious to see if IRF3 contributed to inflammasome priming and activation. The effect of IRF3 perturbations on IL1β induction and inflammasome activation have not been tested in the CNS. Surprisingly, we could not detect the hallmark features of inflammasome activation in the cortical samples of the acute LPS or 4 day LPS challenged WT mice (Supplementary Fig. 2B, C). LPS-mediated inflammasome activation has also been reported before in the hippocampus [32]. Therefore, we evaluated hippocampal lysates of the 4 day LPS challenged mice for inflammasome activation. Indeed, we found increased levels of pro- and cleaved-IL1β indicating inflammasome priming and activation in the WT-LPS group compared to the WT-saline mice. This increase in pro- and cleaved- IL1β levels was significantly attenuated in the IRF3KO-LPS group compared to the WT-LPS group (Fig. 4H, J). This data revealed a novel role of IRF3 in inflammasome activation in the CNS as well as in regional sensitivity to LPS-mediated inflammasome activation.

Together, this data complements the observations in our acute LPS model and suggests that IRF3 deletion provides protection against various proinflammatory features of repeated LPS challenges such as myeloid cell infiltration, astrocyte proliferation, and inflammasome activation.

Expression of a constitutively active form of IRF3 is sufficient to induce neuroinflammation

Phosphorylation of two serine residues (S388/390) is critical for IRF3 activation and nuclear translocation [19]. Previously a constitutively active form of IRF3 i.e. IRF3-2D (S388D/S390D) was shown to induce proinflammatory cascade in macrophages and adipocytes [23]. Thus, to specifically determine the effects of IRF3 activation in microglia, we expressed IRF3-2D in microglia using $Cx3cr1Cre^{ERT2}$ and IRF3-2D-Lox mice.

We confirmed the expression of IRF3-2D constructs in EFYP + cells from the brain at the transcript and protein levels (Supplementary Fig. 4A, B). We observed the characteristic protein doublet for IRF3-2D in $EYFP^{+}$ cells [23] (Supplementary Fig. 4B).

Similar to previous reports with $Cx3cr1Cre^{ERT2}$ mice, we observed leaky expression of IRF3-2D in the absence of tamoxifen and a strong trend in further increase with tamoxifen administration (supplementary Fig. 4A, B) [33]. Therefore, we have also included additional Cre_only controls (Cre_Tam/Oil). Cre_Tam and Cre_Oil groups were very similar and thus data is pooled as a single group referred to as Cre_only.

$Tmem119^{+}$ microglia from tamoxifen-administered IRF3-2D_Cre group (hereafter referred as IRF3-2D,Cre_Tam) (Fig. 5A–D) showed significant morphological changes with reduced branching and intersections, compared to the IRF3-2D,Cre_Oil or Cre_only group suggestive of a reactive microglia morphology (Fig. 5A,C,D). The morphological changes in the branching did not lead to the changes in cell volume (Fig. 5B).

Moreover, flow cytometry of IRF3-2D,Cre_Tam brain samples revealed a distinct $EYFP^{+}$ $CD11b^{+}CD45^{high}$ population of infiltrating monocytes in addition to $Cd11b^{+}CD45^{intermediate}$ microglia population (Fig. 5E, F, G). This data corroborates the critical role of IRF3 in

(See figure on next page.)

Fig. 3 Transcripts from microglia & astrocytes of IRF3KO mice show a dampened proinflammatory response to LPS. **A** Schematic of the protocol for isolation of microglia and astrocytes after acute LPS challenge. **B**–**H** Quantification of qRT-PCR of transcripts from microglia show increased transcript levels of *Ifit1*, *Isg15*, *Gbp2*, *H2-D1*, *and Cox2* in WT-LPS group. While IRF3KO mice do not show significant induction of ISGs and certain proinflammatory transcripts in microglia (**B**–**F**), they appear more sensitive to LPS-mediated induction of *C3* transcripts (**G**). Also, compared to WT, IRF3KO microglia show a similar reduction in levels of *P2ry12* (**H**). N = 6,9 per group. **I**–**L** Quantification of qRT-PCR of transcripts *(Ifit1*, *Gbp2*, *Igtp*, *Gfap)* from astrocytes shows the attenuated response to LPS-induced transcripts compared to the WT controls. N = 7,9 per group. Two-way ANOVA with Tukey's multiple comparisons. *p < 0.05, **p < 0.01, ***p < 0.001, ****p < 0.0001

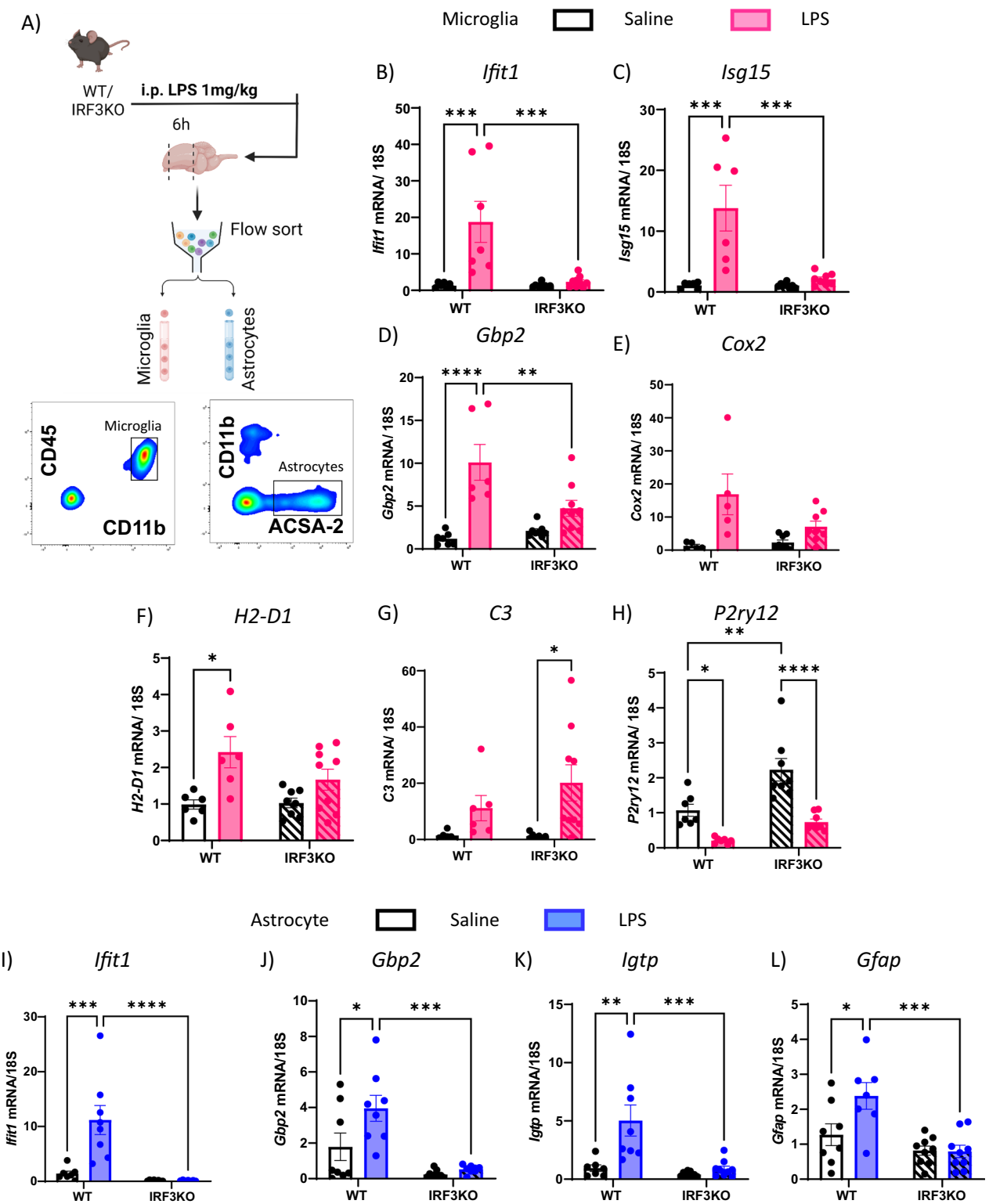

Fig. 3 (See legend on previous page.)

LPS-induced myeloid cell infiltration in the brain discussed earlier (Fig. 4B,C). Moreover, the expression levels of CD45 and CD11b were elevated in the microglia population (gated on the $Cd11b^{+}CD45^{intermediate}$) of IRF3-2D, Cre_Tam mice compared to that of Cre_only mice (Fig. 5H, I) further validating the proinflammatory microglia phenotype of IRF3-2D, Cre_Tam group.

Additionally, IRF3-2D, Cre_Tam mice also showed astrocyte reactivity in the cortex, suggesting that IRF3 activation is sufficient to mediate astrocyte reactivity (Fig. 5J, K).

Taken together, these results demonstrate a proinflammatory role of IRF3 in microglia and astrocytes.

Despite this evidence of neuroinflammation, we found no significant behavioral changes in neither of the anxiety tests (i.e. open field test and elevated plus maze) nor the Y-maze test, (Supplementary Fig. 5A–C) in the IRF3-2D,Cre_Tam mice compared to IRF32D,Cre_Oil or Cre_only group.

To gain deeper insights into the proinflammatory profile of IRF3-2D expressing cells, we performed bulk-RNA sequencing on flow sorted $Cx3cr1^{+}(EYFP^{+})$ population of myeloid cells from the brain (cortex, subcortical areas, and hippocampus).

To account for changes induced by tamoxifen administration, we compared the transcriptome of IRF3-2D, Cre_Tam $EYFP^{+}$ population with that of Cre_Tam. We observed in total 908 genes that were differentially regulated in response to the presence of IRF3-2D. The expression of IRF3-2D in microglia resulted in a proinflammatory transcriptome enriched with the pathways related to IFN-β, IFN-γ, and viral responses (Fig. 6A, B, Table 1). In addition, we observed upregulation of pathways related to leukocyte migration, and cell adhesion further strengthening the effect of IRF3 on myeloid cell infiltration observed in this study (Figs. 4B,C & 5E,F,G). We also found upregulation of pathways related to antigen presentation and co-stimulatory molecules *[H2 (-Ab1, -Eb1, -Aa, -Q6, -Q7, -K1, -D1, -Q5, -M3, -Dma, -K2, -T22, -Q4), Tap1, Cd74, Cd40, Cd72)*, immunoproteasome (*Psmb9, Psme1, Psme 2*), cytoskeletal reorganization and ER-phagosome, providing further insights into the proinflammatory role of IRF3.

The top differentially regulated genes in this comparison were the subset of genes associated with AD. These included genes such as *Apoe, Axl, Cd74, Fth1, Itgax, and Ctsb* (Fig. 6B). *As Apoe*, was the top candidate, we validated its expression at the protein level. We observed that APOE expression was significantly upregulated in $Tmem119^{+}$ microglia in IRF3-2D,Cre_Tam group compared to IRF3-2D,Cre_Oil or Cre_only group (Fig. 6C,D).

Microglia from the AD and neurodegenerative models show particular gene signatures which are termed as activated response microglia (ARM), or disease associated microglia (DAM) or microglia neurodegenerative phenotype (MGnD) with overlapping features [14, 34–36]. In addition, interferon-responsive microglia i.e. IRMs have also been reported in AD and aged mouse brains [14, 16]. Therefore, we wondered what proportion of $EYFP^{+}$ cells from IRF3-2D animals showed gene signatures associated with IRMs and AD. We performed data deconvolution with single-cell RNA seq data to determine the cell fractions in IRM and ARM-like cells [14]. The presence of IRMs was observed in IRF3-2D,Cre_Tam mice (Fig. 6E) in line with the increased interferon signaling observed (Fig. 6A). Interestingly, we observed significantly increased population of ARM in IRF3-2D,Cre_Tam group compared to the Cre_only group, and a strong trend in increase ($p < 0.09$) compared to IRF3-2D_Oil group (Fig. 6E). IRF3-2D,Cre_Oil group also showed presence of IRM and increasing trend in ARM population compared to the Cre_only controls, reflecting on the leaky expression of IRF3-2D and associated proinflammatory signaling in this model (Fig. 6E, Supplementary Fig. 6, Table 1). Nonetheless, these results show that IRF3-mediated signaling is sufficient to induce IRM and ARM signatures in microglia.

(See figure on next page.)

Fig. 4 IRF3KO mice show reduced proinflammatory changes in the brain after repeated LPS challenges. **A** Schematic of the 4 day repeated LPS challenge paradigm. **B** Representative images of FACS analysis showing presence of significantly more infiltrating myeloid cells in Quadrant 2 (Q2)($CD11b^{+}$,$CD45^{high}$) in the WT-LPS group in addition to the microglia population ($CD11b^{+}$,$CD45.^{intermediate}$) in Q3. **C**-**D** Quantification of the percentage and absolute cell count of infiltrating cells shows that LPS-induced infiltration of myeloid cells was markedly reduced in the IRF3KO-LPS mice compared to the WT-LPS. N = 5,6 each group. The parent population is defined as live cells based on DAPI staining. **E**–**F** Quantification of the levels of mean fluorescence intensity of CD11b gated on the microglia in Q3 shows a more significant increase in WT-LPS microglia compared to IRF3KO-LPS microglia. N = 5,6 each group. **G**, **I** Representative images of western blots showing increased astrocyte proliferation in LPS-treated WT and IRF3KO samples in the cortical lysates. Quantification shows that the extent of astrocyte proliferation is significantly lower in IRF3KO mice compared to the WT. N = 9,10 each group.**H**, **J** Representative images and quantification of western blots showing a significant increase in the hippocampi of pro-IL1β (full length) and cleaved-IL1β indicate activation of inflammasome in LPS-treated WT samples. Quantification shows that IRF3KO mice are protected from this increase. N = 9,10 each group. Two-way ANOVA with Tukey's multiple comparisons. *$p < 0.05$, **$p < 0.01$, ***$p < 0.001$, ****$p < 0.0001$

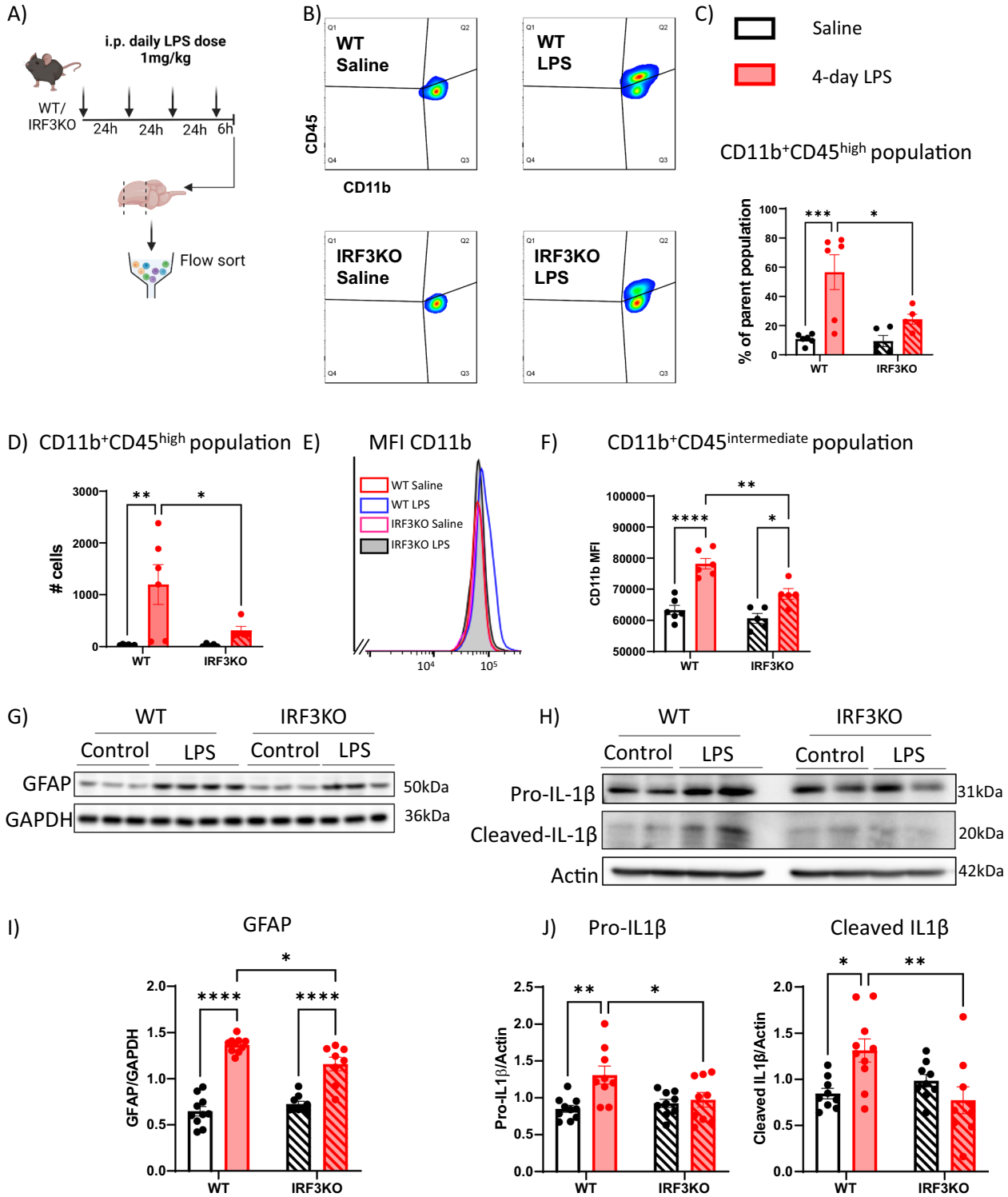

Fig. 4 (See legend on previous page.)

Because these results indicated a role of IRF3 in AD pathology, we directly tested the recruitment of IRF3 in AD by stimulating WT microglia with synthetic Aβ oligomers. We observed significant IRF3 phosphorylation after 24 h of Aβ stimulation (Fig. 6F, G). Thus, we conclude that IRF3 plays a critical role in microglia-mediated

proinflammatory responses and regulates signaling relevant in AD.

Expression of ZBP1, a target of IRF3, is upregulated in microglia in various neuroinflammatory conditions

To further dissect the molecular mechanism and genes regulated by IRF3 signaling in microglia beyond LPS challenge or IRF3-2D model, we compared the transcriptome of IRF3-2D overexpressing EYFP^{+} cells to that of microglia from various neuroinflammatory conditions such as AD (5XFAD), Tauopathy model, LPS challenge, and glioma [37]. In each data set, we used differentially upregulated genes showing a Log fold change of > 0.6 and adjusted p-value of < 0.05. From these comparisons, we identified 10 genes, comprising direct and indirect targets of IRF3, that are of relevance across different neuroinflammatory conditions (Fig. 7A). IRF3-mediated changes in the transcriptome primarily result from the direct transcriptional activity of IRF3 or IRF3-mediated secondary signaling cascades. The direct transcriptional targets of IRF3 have been previously identified by 'Cleavage Under Targets and Release Using Nuclease' (CUT and RUN) technique from hepatocytes expressing IRF3-2D [22]. Of these 10 common genes, 3 genes were identified as direct transcriptional targets of IRF3- *Oasl2, Zbp1 and Tlr2* by CUT and RUN [22].

In view of the novelty, we particularly focused on ZBP1. ZBP1 was initially recognized as interferon-inducible tumor-associated protein [38]. ZBP-1 is shown to be critical for LPS-mediated production TNFα and IFNβ in macrophages [39]. However, the role of ZBP1 in neurological disorders remains poorly studied. Thus, we aimed to validate ZBP1 as the target of IRF3 in our models of LPS challenge in the CNS.

We observed that there was a striking increase in the expression of Zbp1 (~ 2.5 fold) in WT microglia cultures treated with LPS for 6 h, which was absent in IRF3KO primary microglia (Fig. 7B). Similarly, after the in vivo acute LPS challenge, *Zbp1* mRNA was significantly induced in microglia and astrocytes isolated from the WT-LPS group, while no change could be detected in cells isolated from the IRF3KO mice (Fig. 7,C, D). This data corroborated results from the in vivo 4-day repeated LPS challenge model, where only the WT, and not the IRF3 deficient, brain tissue showed significantly elevated levels of ZBP1 after LPS treatment (Fig. 7E). To test the validity of these findings in AD models, we assessed ZBP1 expression in primary microglia cultures stimulated with Aβ for 24 h. We observed a significant reduction in Aβ -mediated increase in ZBP1 in IRF3KO cultures compared to the WT (Fig. 7F, G).

Thus, together we identify ZBP1 as a novel proinflammatory target common across different neuroinflammatory conditions and show that ZBP1 expression is regulated by IRF3-induced signaling in microglia and astrocytes.

Discussion

The function of IRF3 has been extensively studied in peripheral models of TLR3 and TLR4 activation i.e. viral and bacterial infection, respectively, including our work on IRF3 in sterile inflammatory conditions such as alcohol abuse and obesity [23, 24, 40]. In the CNS, the role of IRF3 has been studied in viral encephalitis. Phosphorylation deficient mutation at S386 of IRF3 is associated with reduced IFN-I signaling in Herpes simplex encephalitis (HSE) patients [41]. IRF3KO mice showed higher mortality rates and increased inflammation on HSE infection [42]. Similarly, IRF3 deficient mice showed inability to resolve inflammation in the CNS by alphavirus infection [43]. In this report we evaluated the cell type-specific contribution of IRF3 in microglia and its impact in a broader context of neuroinflammation.

(See figure on next page.)

Fig. 5 Expression of a constitutively active form of IRF3 in Cx3cr1^{+} cells in the brain is sufficient to induce neuroinflammation. **A** Representative images of microglia (Tmem119^{+} cells were picked) co-stained with Iba1 and Sholl analysis performed using filament tracer software from Imaris. The scale bar is 21 µM. **B** Total volume of the cells did not change between any of the groups tested. **C** Quantification of the microglia morphology shows that microglia (Cells positive for Tmem119) from IRF3-2D,Cre_Tam group show significantly reduced branching compared to IRF3-2D,Cre_Oil and Cre_only groups. **D** Microglia from IRF3-2D,Cre_Tam group show reduced number of intersections at 10–30 µm compared to that of IRF3-2D,Cre_Oil and Cre_only groups. * represents comparison with Cre_only, # represent comparison with IRF3-2D,Cre_Oil. For Sholl analysis N=6-8 for each group. >7 microglia were analyzed per animal. Data was analyzed using One-way ANOVA. *p<0.05, **p<0.01, ***p<0.001, ****p<0.000. **E**-**G** Representative images and quantification of FACS analysis showing the presence of infiltrating myeloid cells (CD11b^{+},CD45^{high}) in the IRF3-2D,Cre_Tam (Yellow arrow) group in addition to the microglia population (CD11b^{+},CD45^{intermediate}) (White arrow). **F** Shows the quantification as % of the parent population, while **G** shows absolute number of infiltrating cells. N= 8,9 each group. One-way Anova with Sidak's multiple comparison test. ****p<0.0001.**H**-**I** Quantification of CD45 and CD11b MFI gated on microglia (White arrow in E) shows significant upregulation in IRF3-2D,Cre_Tam, suggesting more reactive state compared to Cre_only controls. N= 8,9 each group. One-way Anova with Sidak's multiple comparison test. ****p<0.0001. **J**-**K** Quantification of the western blots shows proliferation of astrocytes, as measured by GFAP levels in cortical lysates, of IRF3-2D,Cre_Tam compared to Cre_only. N= 6,7 each group. Kruskal-Wallis test with Dunn's multiple comparison test. **p<0.01

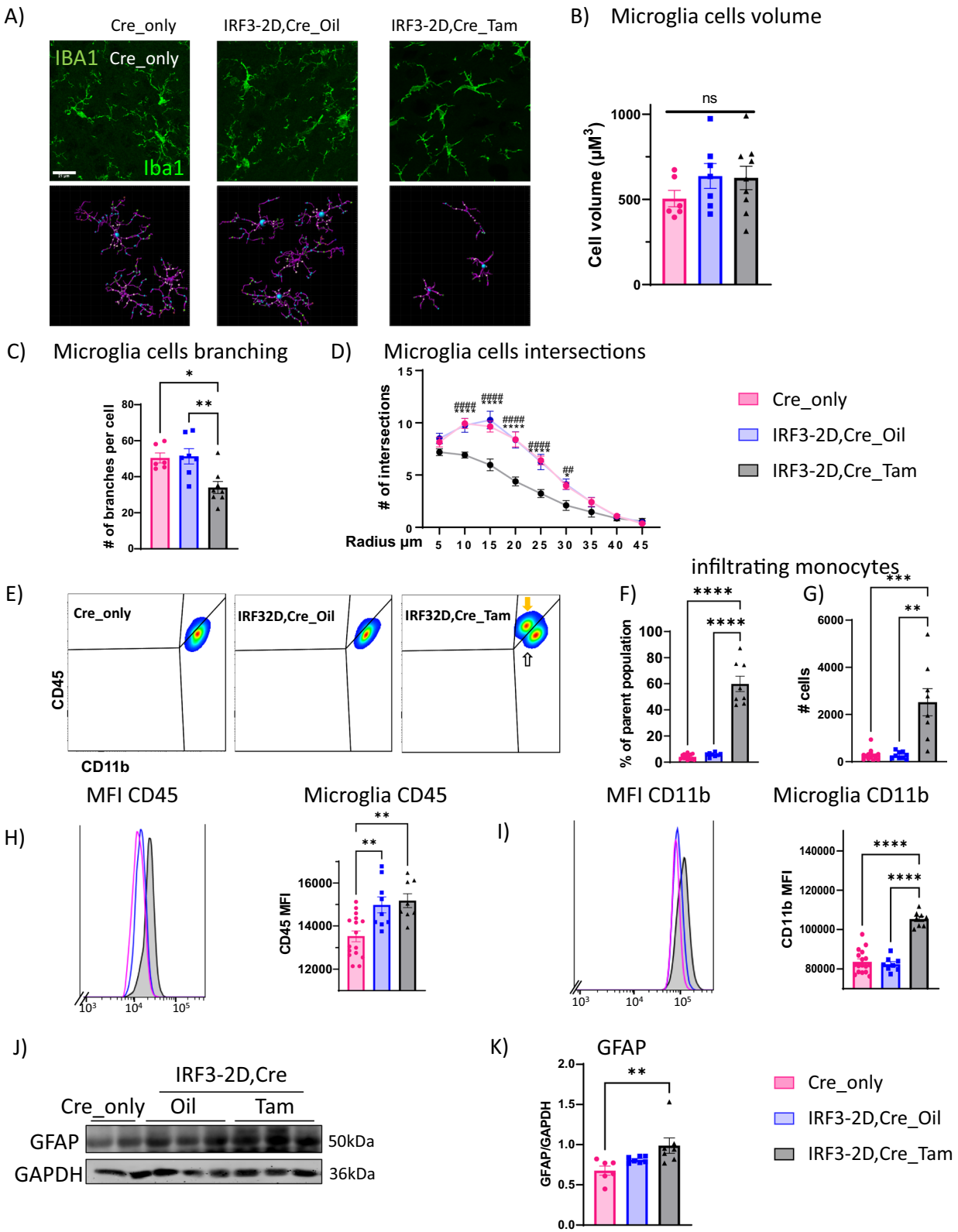

Fig. 5 (See legend on previous page.)

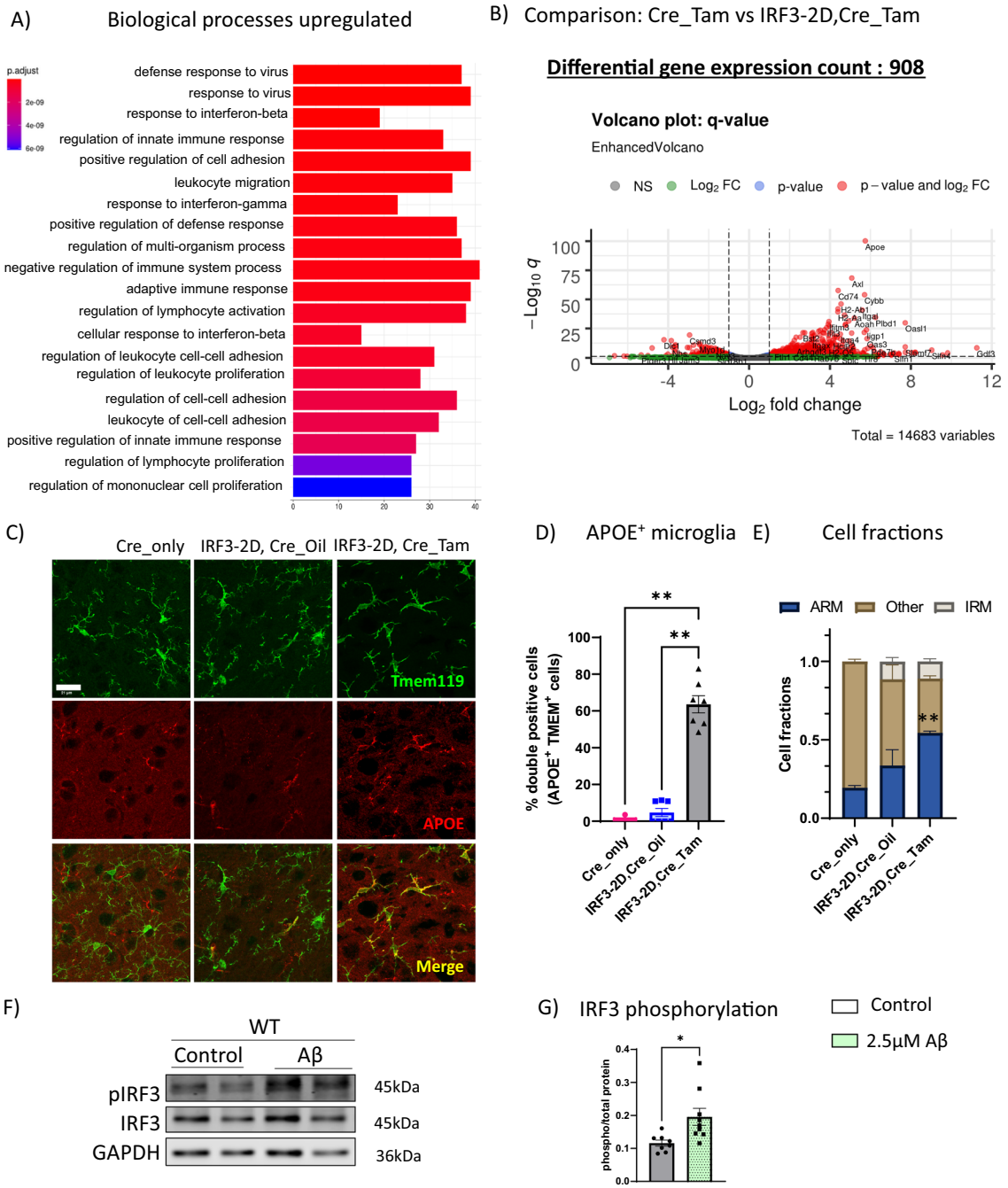

Fig. 6 Overexpression of a constitutively active form of IRF3 leads to proinflammatory phenotype and induces expression of the AD risk genes. **A** GO analysis of the differentially upregulated genes in FACS-sorted myeloid cells from IRF3-2D,Cre_Tam mice compared to Cre_only show proinflammatory phenotypes and upregulation of pathways related to interferon-β, γ signaling, cell adhesion, and leukocyte proliferation. **B** Volcano plot showing differentially expressed genes in IRF3-2D,Cre_Tam mice compared to Cre_Tam. Note the upregulation of AD-associated genes. (n = 2 for Cre_Tam, n = 3 for IRF3-2D,Cre_Tam). **C**-**D** Representative images of APOE staining in the cortex. Quantification confirms that APOE levels are significantly upregulated in the microglia from IRF3-2D,Cre_Tam group. The scale bar is 21 μM. N = 6,8 per group. One-way Anova with Sidak's multiple comparison test. **p < 0. 01. **E** Deconvolution analysis on myeloid cells from IRF3-2D,Cre_Tam mice shows significantly more ARM-like cell fraction compared to Cre_only fraction. Both IRF3-2D,Cre_Oil and IRF3-2D,Cre_Tam cells contain IRM- populations in response to IRF3-2D-mediated signaling. **F**-**G** Western blot image and quantification of cell lysates from primary WT microglia treated with Aβ oligomers (2.5 μM) for 24 h, show significant IRF3 phosphorylation. N = 8,9 each group. Student's t-test with Welch's correction. *p < 0.05

In addition to TLR4/3 signaling, various inflammatory signaling cascades culminate on IRF3 activation. IRF3 can be activated intracellularly by cytosolic DNA generated by DNA damage response or microbial invasion [44, 45]. Also, we have shown before that IRF3 can be activated via endoplasmic reticulum stress through STING [40]. cGAS-STING activation is observed in various neuroinflammatory conditions such as AD,TBI, Parkinson's disease (PD), aging etc. indirectly implicating IRF3 in these conditions and emphasizing the need to study functions of IRF3 in the CNS [6, 7, 46, 47].

In this manuscript, we demonstrate that the expression of IRF3 in microglia is important in three different neuroinflammatory contexts; LPS-TLR4 signaling, Alzheimer's disease-Aβ mediated neuroinflammation and IRF3-2D: stimulus independent IRF3 activation. Moreover, we showed that IRF3 activation and IRF3-mediated signaling is sufficient to drive the expression of AD-related genes.

Activation of TLR4, a widely studied pattern recognition receptor, has been observed in a myriad of neuropathologies ranging from gram-negative bacterial infections (mimicked here by LPS), AD, PD, MS and amyotrophic lateral sclerosis (ALS) [48–51]. TLR4 also senses both pathogen-associated molecular patterns, such as LPS, and sterile inflammatory signals, for example HMGB1 [52, 53]. Furthermore, LPS primes brain responsiveness to HMGB1 [54]. TLR4 triggers two downstream pathways through adaptor proteins: MyD88 and TRIF dependent leading to MyD88 independent signaling [55]. While much attention is paid to MyD88-dependent or NF-κB-mediated signaling, here we highlight the role of IRF3 in MyD88-independent TLR4 signaling.

To study the role of IRF3 in LPS-TLR4 signaling in vivo we used the 6 h acute LPS model. We observed that IRF3 is involved in the production and release of the key inflammation-associated cytokines and chemokines, sickness behavior as well as Type 1 interferon-dependent genes in the brain. Other mediators, such as TNFα and IFNβ also contribute to sickness behavior, however, we could not detect a significant amount of these cytokines in the cortex of mice at 6 h post LPS stimulation when other markers were assessed in our experiments [26, 56].

Next, we ascertained the cell type-specific role of IRF3 by using primary cultures and flow-sorted microglia. In primary microglia we observed that IRF3 deletion directly modulated the signaling events downstream of TLR4 particularly in the first 30 min compared to 120 min, suggesting that effects of IRF3 deletion are partially compensated by the feedback loops between secondary messengers downstream of TLR4 signaling. The in vitro results emphasized the importance of IRF3 in microglia intrinsic signaling in the absence of communication from other CNS or peripheral cell types.

In flow-sorted microglia of WT and IRF3KO mice, the LPS-induced upregulation of proinflammatory transcripts showed partial dependence on IRF3. Surprisingly, we observed complement factor *C3* transcripts were upregulated in IRF3KO-LPS microglia compared to WT-LPS groups. This finding is surprising since *C3* is a known target of IFN-I [4] and is also significantly upregulated in IRF3-2D expressing myeloid cells (Fig. 6B). A compensatory effect of LPS-mediated IRF3-independent pathway of complement activation may explain this effect [57]. Moreover, microglia transcripts from IRF3KO mice showed elevated levels of the homeostatic marker *P2ry12* compared to the WT. However, solely based on this result it is difficult to draw conclusions on the homeostatic state of microglia in these mice. Analysis of the transcriptome of IRF3KO mice microglia may shed light on this aspect.

In neuroinflammatory diseases there is continued presence of disease associated molecular patterns (DAMPs) and/or PAMPs that sustain inflammation. Thus, we also tested a four-day model of repeated LPS stimulations where we discovered a novel role of IRF3 in monocyte infiltration and inflammasome activation in the CNS. The IFN response in the CNS has been associated with myeloid cell infiltration under tumorogenic conditions and viral infections [31, 58], however, the specific

(See figure on next page.)

Fig. 7 *Zbp1* is a proinflammatory transcript common across various neuroinflammatory conditions and its expression is regulated by IRF3. **A** An upset plot of differentially expressed genes in IRF3-2D expressing myeloid cells and microglia from various neuroinflammatory conditions. The number of differentially upregulated genes from each disease are represented in the bracket. Note the set of common genes across all five neuro-inflammatory conditions encased in blue. Underlined genes were identified as direct transcriptional targets of IRF3. **B** Representative image and quantification of western blot from microglia cultures treated with LPS for 6 h show 2.6 fold induction in ZBP1 in WT microglia but not IRF3KO cultures. N = 3 biological replicates. Unpaired t-test. *p < 0.05. **C**, **D** Quantification of qRT-PCR of microglia and astrocytes sorted from acute LPS model (6 h LPS challenge in vivo) shows upregulation of Zbp1 mRNA in WT, which is absent in IRF3KO condition. N = 6–9 in each group. Two-way ANOVA with Tukey's multiple comparisons. **p < 0.01, ****p < 0.0001. **E** Western blot image and quantification of cortical tissue from WT and IRF3KO mice treated with LPS or saline for 4 days, show ZBP1 induction only in the WT-LPS group and absent in IRF3KO-LPS condition. N = 9,10 each group. Two-way ANOVA with Tukey's multiple comparisons. ****p < 0.0001. **F**, **G** Western blot image and quantification of cell lysates from primary WT microglia treated with Aβ oligomers (2.5 μM) for 24 h, show significant ZBP1 induction on treatment with Aβ. There is significant attenuation of Aβ-induced ZBP1 induction in IRF3KO microglia compared to the WT group. N = 8,9 each group. Student's t-test with Welch's correction. *p < 0.05

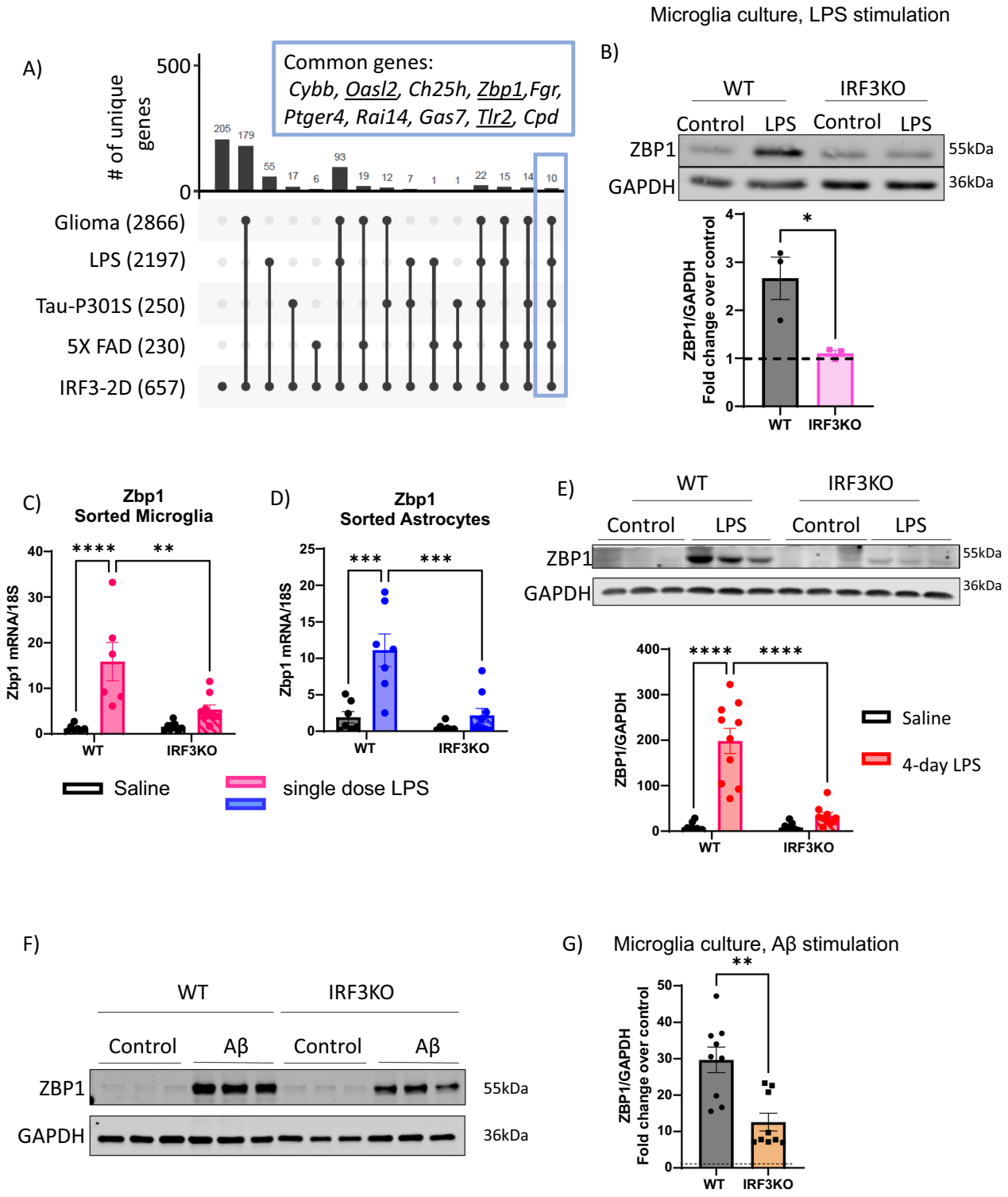

Fig. 7 (See legend on previous page.)

role of IRF3 in myeloid cell infiltration in the brain has not been described previously. The reduced myeloid cell infiltration observed in the IRF3KO-LPS group in the 4-day model correlates with the reduced levels of MCP1 seen in the acute model in Fig. 1C. Interestingly, at 4 day time point, we could not detect MCP1 anymore in the

samples, suggesting that MCP1 release in the initial LPS challenge is sufficient to elicit myeloid cell infiltration in the brain.

In our study, reduced NLRP3 inflammasome activation modulated by IRF3 deletion in the CNS was another novel finding. This observation is significant in light of the critical role of NLRP3 in AD, and other neurological disorders [59, 60]. This result is in line with the previous observations made by our lab and others showing reduced NLRP3 inflammasome activation in the absence of IRF3 in the peripheral models of inflammation [24, 61].

IRF3 is expressed in the brain by microglia, astrocytes, neurons, endothelial cells and oligodendrocytes [30]. As astrocytes have increasingly gained importance to partake in regulating immune responses in the brain, we assessed the responses from astrocytes. Indeed we found a significant reduction in the LPS-induced proinflammatory response of astrocytes in the absence of IRF3 expression in both the in vivo models of LPS that we tested, suggesting a major role for IRF3 in astrocyte responses to acute as well as repeated LPS challenges. Proinflammatory responses of microglia contribute to astrocyte activation, however, in our study we cannot distinguish between microglia dependent or astrocyte autonomous role of IRF3 in LPS-mediated astrocyte activation [17, 62].

While our data in IRF3KO mice and cells indicated the importance of this pathway in TLR4-mediated neuroinflammation [21, 40, 44, 63], [64, 65] next, to understand the isolated effects of IRF3 activation in microglia we took advantage of the IRF3-2D-lox line, described previously [23]. Our data indicate that constitutive IRF3 activation in microglia results in key features of neuroinflammation including increased monocyte infiltration to the brain and increased GFAP expression suggesting astrocyte activation. We also found that a key feature of IRF3-2D expression was the upregulation of certain DAM genes, or ARMs, most notably *Apoe*. *Apoe* is a major risk factor for the late-onset Alzheimer's disease. In addition, *Apoe* expression in microglia has been shown to regulate microglia immunometabolism influencing their ability to respond to Aβ plaques, and tauopathy [34, 66–68]. APOE-TREM2 pathway has been shown to be important for expression of DAM and ARM genes [14, 34]. Our model of IRF3-2D, suggests that sustained IRF3 activation is sufficient to drive the expression of *Apoe*, which in turn can regulate the expression of certain genes associated with microglia phenotype in neurodegenerative diseases. *Apoe* is not one of the known transcriptional targets of IRF3; our study suggests that it may be upregulated through IRF3-mediated mechanisms. Further investigation is needed to determine the exact mechanism of IRF3-mediated upregulation of APOE.

Since the bulk RNAseq performed from IRF3-2D,Cre_Tam mice comprises $EYFP^+$ cells in the brain i.e. microglia and infiltrating myeloid cells, we ascertained microglia specific effects by visualizing $Tmem119^+$ cells for morphological analysis (Fig. 5A), and APOE expression (Fig. 6C) and using $CD11b^+CD45^{intermedate}$ gate for assessing levels of CD11b in Fig. 5E,F). We also compared the transcriptome of $EYFP^+$ cells devoid of infiltrating myeloid cells from IRF3-2D,Cre_Oil with Cre_Oil groups (Supplementary Fig. 6). This comparison showed a total of 321 differentially regulated genes (DEGs), fewer than the 908 DEGs described in IRF3-2D, Cre_Tam group in Fig. 6. Here, we observed proinflammatory pathways and genes such as *Axl, Cybb, Cst7, H2-D1, Cd74* (Supplementary Fig. 6) and an increasing trend in ARM fraction (Fig. 6E), collectively showing a proinflammatory effect of IRF3-2D activation on microglia in the absence of infiltrating myeloid cells.

While these results clearly establish effects of IRF3-2D on microglia, we cannot rule out the effect of leaky expression of IRF3-2D in $Cx3CR1^+$ myeloid cells in the periphery and further experiments would be needed to tease those apart. It is interesting to note that Tamoxifen administration further increased the ARM-like fraction in IRF3-2D, Cre_Tam group while the IRM-like fraction shows no additive effect, it is possible that the expression of ARM related genes is induced by targets of IRF3 not directly involved in IFN-I signaling (CUT and RUN analysis [22]).

IFN-I signaling in early postnatal microglia or during embryonic development has been associated with increased anxiety [9, 69]. IFN-I in adults is associated with social interaction deficits, and poor memory performance in mouse models of TBI, AD [5, 70, 71]. On the contrary treatment with IFNβ in MS patients is associated with improved cognitive behavior [72, 73] suggesting that effects of IFN-I signaling on behavior can be context dependent. We found no obvious behavioral changes in the anxiety or memory performance of IRF3-2D mice. These mice were assessed for behavior, 5 weeks after tamoxifen treatment thus we cannot rule out the development of any compensatory or tolerogenic behavioral and transcriptional changes that may mask the subtle underlying behavioral abnormalities. Moreover, in this model we see IRF3-mediated signaling which may not recapitulate the full spectrum of inflammation and IFN-I signaling observed by others. Also, we have assessed only a specific set of behavioral features and more thorough investigation using a battery of tests for social and cognitive animal behavior will be needed to ascertain the effect of IRF3 activation on rodent behavior.

In view of the data from our IRF3-2D models and the literature, we investigated the relevance of IRF3 signaling in cellular models of Aβ. Indeed, we observed significant IRF3 phosphorylation in response to Aβ. It is of important to note that the upstream signaling cascades that result in IRF3 activation in response to LPS and Aβ can be different with some overlap. LPS challenge experiment in microglia cultures shows IRF3 phosphorylation (Fig. 2A) likely through MyD88 independent pathway as expected by the previous studies performed in bone marrow-derived macrophages following LPS challenge [21]. 1000×higher LPS concentrations (~10 µg/mL and above) than our assays have shown induction of DNA damage response in epithelial cells or macrophages after 24 h of LPS treatment [64, 65]. Aβ and Tau responses are governed by both -DNA damage-cGAS-STING and TLR4-dependent signaling [74–76]. Further investigation using gene-specific knockouts or pathway-specific inhibitors would be needed to determine the specific contribution of each.

Lastly, to evaluate the presence of signatures of IRF3 activation and IFN-I signaling in different proinflammatory disorders, we compared the genes upregulated with IRF3-2D expression to that of the genes upregulated in different neuroinflammatory disorders such as glioma, AD model of amyloid and tauopathy, and LPS challenge. Of these 10 common genes, we were particularly interested in ZBP1. ZBP1 is known for its function in cell death pathways, viral response and inflammasome activation [38]. In addition, the role of ZBP1 in proinflammatory signaling, independent of cell death, is also emerging [77]. However, there are limited studies investigating the role of ZBP1 in neuroinflammation and its role in AD is beginning to emerge [78].

Previous studies have shown ZBP1 to be a regulator of IRF3 [39]. We recently showed that ZBP1 expression is modulated by IRF3 in mouse models of cholestatic-liver injury [24]. Here we show for the first time that IRF3 can directly regulate ZBP1 levels in microglia and astrocytes. Importantly, we also showed that Aβ challenge induced ZBP1 expression in an IRF3 dependent fashion, strengthening the pro-inflammatory role of IRF3 in AD related pathology. Detailed investigation of the role of IRF3 in AD will emerge from Amyloid and Tau-based in vivo models.

In this manuscript, we elucidated pathways that lead to IRF3 activation, and further research is needed to dissect the specific role of various effectors downstream of IRF3 activation. Canonically, IRF3 activation stimulates IFN-I receptor signaling resulting in STAT-1 signaling and ISGs production [79]. ISGs such as *Isg15, IFP35*, have been associated with neurological disorders including AD, Aicardi-Gtières syndrome, MS, PD and ALS [4, 7, 80–84]. Moreover, *Axl*, an ISG, is a microglia receptor implicated in phagocytosis of Aβ [85]. Expression of complement component *C3* is also induced by IFNβ and its expression is highly relevant in microglia-mediated synaptic pruning in various neuroinflammatory conditions [86, 87]. Assessment of these IRF3 effectors using various genetic manipulations will likely reveal novel therapeutic targets.

IRF3KO mice used in this study have been reported to carry a concomitant *Bcl2l12* mutation [25]. Importantly, IFN-I responses, in MEFs derived from these mice, are IRF3 specific [88]. In addition, in our manuscript, the use of IRF3-2D mice and the observed IRF3 phosphorylation in WT microglia cultures in response to various stimuli provides a strong support for the role of microglial IRF3 in neuroinflammation. Also, we found no obvious differences in the weight or baseline behavior of these mice. Using conditional IRF3KOs devoid of the *Bcl2l12* deficiency may provide further insights [25].Taken together we discovered new insights into the role of IRF3 in promoting neuroinflammation specifically, in microglia and highlight IRF3 and its downstream genes as important players in various neuroinflammatory conditions.

Methods

Mice: The following mice were used- C57BL/6 from Jax mice (000664), IRF3KO (described previously, [24], Cx3cr1^{CreERT2}(B6.129P2(Cg)-Cx3cr1tm2.1(cre/ERT2)Litt/WganJ-021160), IRF3-2D (C57BL/6-Gt(ROSA)26Sortm4(CAG-Irf3*S388D*S390D) Evdr/J-036261). All strains were in C57BL/6 J background. The mice were maintained on ad-libitum food and water. All the breeding, experiments and euthanasia were conducted as per the institutional IACUC protocol 030-2022. Both males and females between the ages of 3–6 months were used.

Tamoxifen preparation: Tamoxifen stocks of 20 mg/ml were prepared by dissolving Tamoxifen in Corn oil at 37 °C. Mice were given oral gavage 10 mg/kg of Tamoxifen or equal volume oil for consecutive 5 days and used for experiment 5 weeks later.

LPS preparation and administration: LPS was prepared by dissolving LPS in saline at 1 mg/mL and intraperitoneally injected in mice at 1 mg/kg dose as indicated. For in vitro experiments LPS was dissolved in water at 100 µg/mL concentration and diluted in media just before addition.

Microglia and astrocyte flow cytometry: Microglia and astrocytes were flow sorted as described previously [89]. Briefly, mice were transcardially perfused and brains were dissected out. One half of the brains were fixed in 4%PFA overnight. From the other half the prefrontal cortex, hippocampus and cerebellum were dissected out and

frozen on dry ice. The rest of the brain was homogenized in ice-cold HBSS (Ca^{++}, Mg^{++} free). Cells were pelleted at 350 g for 7 min followed by a 37% percoll plus spin without brakes. The top layer of myelin was aspirated and the microglia pellet was washed in HBSS before staining. The cell pellet was incubated in FC block (1:50) at 4 °C for 5 min followed by incubation in antibodies against CD11b, CD45, and ACSA-2 in FACS buffer (2% Fetal Bovine Serum in PBS Ca^{++}, Mg^{++} free) at 4 °C for 20 min. DAPI (1 mg/mL, 1:1000) was added in the last 5 min of antibody incubation. The cells were washed in FACS buffer and sorted using Cytoflex-SRT or analyzed on Cytek Aurora. Microglia were sorted as $Cd11b^{+}$, $CD45^{intermediate}$ population and astrocytes were sorted as $CD11b^{-}$, ACSA-2. For mice in $Cx3cr1^{CreERT2}$ background cells were sorted using EYFP fluorescence. Sorted cells were pelleted and stored at − 80 °C until downstream processing. 15–20 K microglia were used for western blotting. Flow data was analyzed using FlowJo.

Primary microglia cultures: Primary microglia were cultured as described previously with slight modification [90]. Brains from the WT and IRF3KO pups (0–4 days old) were dissected, meninges removed, and homogenized with mortar and pestle. Cells were pelleted by centrifugation at 350 g for 7 min at 4 °C and directly plated onto Poly-D-Lysine (PDL) coated (10 µg/mL) 90 mm dishes. Cells were cultured in DMEMF-12 containing 10% FBS and 1% Penicillin/Streptomycin. Cultures were grown at a standard 5% CO_2, 37 °C incubator. Next day cultures were washed 3 times with phosphate-buffered saline and incubated for an additional 3–4 days in the culture medium described above before the addition of the growth factors (mCSF and TGFβ). 2–3 days later microglia were shaken off the astrocyte monolayer and harvested every 3rd day for 3 cycles. Harvested microglia were plated on PDL coated 12 well dish at 4×10^5 cells per/mL in plain DMEM-F/12 without FBS a day before the experiment. On the day of the experiment, cells were treated with LPS (20 ng/mL) for an indicated amount of time, and supernatant and cells were harvested for further analysis. The supernatant was spun at 10 K for 10 min at 4 °C and stored at − 80 °C until further use. Cells in each well were washed in ice-cold PBS before harvesting. Aβ oligomers were generated as described previously [79].

Western Blotting: RIPA was used as a lysis buffer with a Protease and Phosphatase inhibitor cocktail. Brain tissue was lysed in the tissue homogenizer, followed by a spin at 10 K for 10 min at 4 °C. A predetermined number of cells as indicated above was loaded for western blots from primary microglia cultures or flow-sorted microglia. Total of 50ug of protein was loaded onto SDS gels from tissues. Proteins were transferred onto nitrocellulose membranes and blocked in 5% BSA in 0.1% TBST at room temperature (RT) for 1 h. Blocked membranes were incubated with primary antibodies in 5% BSA overnight and washed 3 times in 0.1% TBST. A secondary antibody was added in blocking solution for 1 h at RT followed by 3 washes in 0.1% TBST before developing the blot.

For western blots from primary microglia in Fig. 2A–E, the results are represented as a comparison between WT and IRF3KO cultures. For signaling cascades the phosphorylation levels are represented as = (LPS-treated [Phospho protein/Total protein])/(Saline-treated [Phospho protein/Total protein]) for WT and IRF3KO cultures separately. Nuclear and cytoplasmic extractions were conducted as per the manufacturer's protocol.

Immunohistochemistry and image analysis: Brains were fixed in 4% PFA overnight, followed by cryopreservation in 30% sucrose solution until the brains sank. Brains were sectioned using Leica cryostat into 25 µm thin sections, collected in 0.05% Sodium Azide solution in PBS, and stored at 4 °C until stained. Desired brains were mounted onto glass slides, washed in PBS and blocked using 1% Triton and 10% Horse Serum in PBS for 1 h at RT. Primary antibodies were dissolved in the blocking and incubated overnight at 4 °C. Primary antibodies were washed at RT in 1% Triton in PBS and incubated in secondary antibodies in 1% Triton and 1% Horse serum for 1 h at RT. After secondary antibody incubation, DAPI (1 mg/ml at 1:1000) solution was added for 5 min at RT followed by 2 washes with 1% Triton in PBS. Sections were imaged at 63×magnification on a Zeiss LSM-700 confocal microscope. Iba^{+} staining was used for morphometry analysis. In Fig. 5A, the sections were co-stained with Tmem119, a microglia specific marker, to verify the microglial identity of the cells. The filament tracer module and Sholl analysis extension in Imaris (Bitplane; Zurich, Switzerland) were used to assess microglia morphometry.

Bulk-RNA seq: 1000 sorted microglia were suspended in 1% beta-mercaptoethanol in TCL buffer and sequenced using smart-seq2 platform at Broad Institute. Briefly, the raw sequencing reads were quality-checked and data were pre-processed with Cutadapt (v2.5) for adapter removal. Gene expression quantification was performed by aligning against the GRCm38 genome using STAR (v2.7.3a). Reads were quantified against Ensembl v98 annotated transcript loci with feature Counts (Subread 1.6.2). Differential gene expression analysis was performed using DESeq2 (v1.24.0) while ClusterProfiler (v3.12.0) was utilized for downstream functional investigations. Plots were generated in R using ggplot2 (v3.3.3), EnhancedVolcano (v1.8.0), ComplexHeatmap (v2.6.2.

For deconvolution analyses we reanalyzed previously published single-cell expression data as described in the

original manuscript (GSE127884). The data containing labels for ARM and IRM cell types was uploaded to the CIBERSORTx platform in order to generate a signature matrix for these cell populations. This matrix was used in combination with our bulk RNA data in order to estimate the relative amounts of each of the cell types. The datasets generated and/or analyzed during the current study are available in Table 1. RNA isolation and qRT PCR: RNA was isolated from microglia and astrocyte pellets using Qiagen RNeasy plus micro kit. cDNA was converted using the Superscript II kit. Gene expression analysis was conducted by qRT PCR using SYBR green from BioRad. Gene expression for every sample was normalized to 18 s rRNA as housekeeping gene.

ELISA: Cytokine levels were detected using ELISA kits. Plates were coated as per manufacturer's instructions. Cell culture supernatant or tissue lysates (prepared as described above) were incubated overnight at 4 °C. Kit-specific protocol was followed for washing and developing of the ELISA plate. Absorbance was measured on a microplate reader and the amount of the cytokine was estimated based on the standard curve.

Animal behavior: Mice were brought into the behavior room 30 min before the experiment. Animal behavior was recorded for 5 min for all tests with an overhead camera and analyzed using Ethovision^{XT}. 20 lx light intensity was maintained in the room. Animal behavior was conducted between 9 am-2 pm. The position of the animal was monitored using the center of mass body point. The behavior tests were performed at least 24 h apart.

For an open field test, 40 cm × 40 cm × 40 cm arena was used. Mice were released in the center of the arena, facing away from the experimenter. As indicated in the figures, the total distance traveled, velocity and time spent in the center were calculated to determine anxiety-like behavior or sickness behavior. The central zone was marked 5 cm away from the walls of the arena.

For the elevated plus maze, mice were released into the central zone facing the open arms away from the experimenter. Total time spent in the open arms was used as the measure of anxiety. The length of each arm was 20 cm.

Y maze test was used to assess memory performance in mice. The Y maze test was performed last, where mice were allowed to explore the arena, and memory was assessed based on the pattern of spontaneous arm alternation. The length of the arms was 15 cm each.

Statistics: Data was plotted as mean ± SEM using GraphPad Prism 9. The appropriate statistical test is indicated in the figure legend for each comparison.

Reagents and resources:

Reagent and resources	Supplier	Catalog number
Antibodies:		
Anti-APOE	Cell signaling technologies	49285
APC anti-mouse/human CD11b [M1/70]	Biolegend	107636
Anti-CD45 rat monoclonal antibody (brilliant violet® 785) [clone: 30-F11]	Biolegend	123109
Anti-Iba1 rabbit polyclonal antibody	Wako chemicals	019-19741
Anti-ACSA-2 antibody, anti-mouse, PE	Miltenyi biotec	130-123-284
Anti-GFAP antibody	Abcam	ab4674
Anti-Iba1 polyclonal guinea pig antibody	Synaptic systems	234 308
Anti-IL1b antibody	GeneTex	GTX74034
Anti-Claudin-1 antibody	Cell signaling technologies	4933
Anti-Occludin antibody	Abcam	ab167161
Anti pNF-kB antibody	Cell signaling technologies	3033
Anti NF-kB antibody	Cell signaling technologies	8242
Anti GAPDH antibody	Proteintech	60004-1
Anti p-P38 antibody	Cell signaling technologies	4511
Anti P38 antibody	Cell signaling technologies	9212
Anti p-ERK1/2 antibody	Cell signaling technologies	4370
Anti ERK1/2 antibody	Cell signaling technologies	9102
Anti-ZBP1, mAb (Zippy-1)	AdipoGen	AG20B001 °C100
Anti pIRF3 antibody 4D4G	Cell signaling technologies	4947
Anti IRF3 antibody D83B9	Cell signaling technologies	4302
Goat anti guinea pig secondary antibody, Alexa Fluor 647	Thermo scientific	A-21450
Goat anti-rabbit secondary antibody, Alexa Fluor 488	Thermo scientific	A11008
Goat anti-mouse secondary antibody, Alexa Fluor 546	Thermo scientific	A-11030

Reagent and resources	Supplier	Catalog number
Rat anti-mouse CD16/CD32 Fc Block	BD pharmingen	553142
Poly-D-lysine hydrobromide,mol wt 70,000–150,000	Sigma-Aldrich	P0899-10MG
Softwares:		
EthoVision	Noldus	Ethovision XT
(Base license plus the multiple body points module)		
FlowJo	FlowJo	
ImageJ	National institute of health	
Imaris	Bitplane	
Reagents		
Lipopolysacchrides	Sigma-Aldrich	L4391
Tamoxifen	Sigma-Aldrich	T5648
Percoll PLUS	GE healthcare	17-5445-02
RNeasy plus micro kit	Qiagen	74034
IL1-α ELISA Kit	R & D systems	DY400
IL-1β ELISA Kit	R & D systems	MLB0°C
MCP-1 ELISA MAX™ Deluxe ELISA Kit,	BioLegend	432704
Mouse IL-6 DuoSet ELISA	R & D systems	DY406
Mouse CXCL1/KC DuoSet ELISA	R & D systems	DY453
Mouse TNF-α DuoSet ELISA,	R & D systems	DY410
IFNβ ELISA kit	R & D systems	MIFNB0
DMEM/F-12, no phenol red	Thermo scientific	21041025
Recombinant human TGF-b	Peprotech	100–35
Mouse colony-stimulating factor-1	Peprotech	315–02
Protease/phosphatase inhibitor cocktail (100X)	Cell signaling technology	5872S
Applied biosystems power SYBR green PCR master mix	Thermo fisher scientific	43-687-02
Iscript™ reverse transcription supermix,	Bio-rad	1708841
Normal horse serum	Vector labs	S-2000-20
Complete, mini, edta-free protease inhibitor cocktail	Roche	4693159001
Aβ	Bachem	H-1368
FITC-Albumin	Sigma-Aldrich	A9771
NE-PER nuclear and cytoplasmic extraction reagents	Thermo scientific	78833

Reagent and resources	Supplier	Catalog number
Primer sequences:	Forward 5′-3′	Reverse 5′-3′
Ifit1/isg-56	GCCTATCGCCAAGATTTAGATGA	TTCTGGATTTAACCGGACAGC
isg-15	GGTGTCCGTGACTAACTCCAT	TGGAAAGGGTAAGACCGTCCT
gbp2	AGATGCCCACAGAAACCCTCCA	AAGGCATCTCGCTTGGCTACCA
cox-2	GCTGTACAAGCAGTGGCAAA	CCCCAAAGATAGCATCTGGA
h2-d1	TGAGGAACCTGCTCGGCTACTA	GGTCTTCGTTCAGGGCGATGTA
c3	CGCAACGAACAGGTGGAGATCA	CTGGAAGTAGCGATTCTTGGCG
p2ry12	CACCTCAGCCAATACCACCT	CAGGACGGTGTACAGCAATG
igtp	CCGTGAACAAGTTCCTCAGGCT	GAGGTCTTGGTGTTCTCAGCCA
gfap	GGA GAG GGA CAA CTT TGC AC	CCA GCG ATT CAA CCT TTC TC
zbp1	GATCTACCACTCACGTCAGGAAG	GGCAATGGAGATGTGGCTGTTG
18 s	GTA ACC CGT TGA ACC CCA TT	CCA TCC AAT CGG TAG TAG CG

Supplementary Information

The online version contains supplementary material available at https://doi.org/10.1186/s12974-024-03203-7.

Supplementary Material 1. Figure 1: IRF3 shows nuclear translocation in microglia in response to LPS stimulus. A–B Representative western blots and quantification shows nearly 2 fold higher IRF3 in the nuclear fraction of microglia stimulated with LPS for 120 min. The purity of the nuclear fraction was verified by the absence of GAPDH. Cytoplasmic fraction was run as a positive control for GAPDH. N=2 in each condition.

Supplementary Material 2. Figure 2: No evidence of myeloid infiltration and inflammasome activation in the cortical sample of mice injected with a single LPS or 4 day repeated LPS challenge. A) Representative images of FACS analysis shows no infiltrating myeloid cells ($CD11b^{+}$,$CD45^{high}$) in the brain in response to 6 h of LPS challenge. Arrow points to the microglia gating ($CD11b^{+}$,$CD45^{intermediate}$). B, C Western blot images and quantification show no significant increase in pro or cleaved form of IL1β 6 h after single LPS (A) (N=4,5) each group or 4 repeated LPS challenges (B) N=9,10 each group. No cleaved isoforms could be detected in any of the conditions.Two-way ANOVA with Tukey's multiple comparisons. *p<0.05, **p<0.01, ***p<0.001, ****p<0.0001

Supplementary Material 3. Figure 3: 4 day repeated LPS challenges do not compromise BBB integrity in WT or IRF3 KO mice. A Representative images of western blots of cortical lysates showing expression of BBB proteins-Claudin-1 and Occludin. B–C Quantification of the western blots shows no differences in levels of Claudin-1 and Occludin either in the WT or IRF3KO tissue lysates. N=9,10 each group. Two-way ANOVA with Tukey's multiple comparisons. *p<0.05, **p<0.01, ***p<0.001, ****p<0.0001. D) Schematic of the BBB permeability assay. E–F Representative images and quantification of areas around the blood vessels show comparable FITC intensities across different treatment conditions. N=3, Two-way ANOVA with Tukey's multiple comparisons. Scale bar is 100μM.

Supplementary Material 4. Figure 4: Increased IRF3 gene count and the presence of a doublet in IRF3 western blot of $EYFP^{+}$ cells from CNS confirms the expression of IRF3-2D construct. A Quantification of the

normalized gene count for IRF3 transcripts from the RNAseq of EYFP$^+$ cells from the brains of mice confirms overexpression of IRF3-2D. IRF3-2D,Cre_Oil mice also showed increased levels of IRF3 transcripts, which were further increased with tamoxifen administration. N=3,4 each group, *p<0.05, **p<0.01, ***p<0.001. One way ANOVA with, Tukey's multiple comparisons. B Western blot and its quantification from flow-sorted EYFP$^+$ cells from IRF3-2D,Cre background shows the presence of a doublet pointed out by arrow indicating the expression of IRF3-2D construct in mice heterozygous for IRF3-2D. Some leaky expression was observed in IRF3-2D,Cre_Oil cells.

Supplementary Material 5. Figure 5: Expression of IRF3-2D in microglia does not cause behavioral changes in mice. A Quantification of % time spent in the center or total distance traveled in an open field arena, showed no difference in any of the genotypes tested. N=6-8 per group. B Quantification of time spent in the open arms was equivalent between all the genotypes tested. N=5-8 per group. C Quantification of % alternation in Y-maze test shows no difference in memory performance in any of the genotypes tested. N=6-8 per group. One way Anova, with Sidak's multiple comparison test.

Supplementary Material 6. Figure 6: Leaky IRF3-2D expression leads to inflammatory transcriptional changes. A Volcano plot showing differentially expressed genes in Cre_Oil vs IRF3-2D,Cre_Oil, with a total of 321 differentially expressed genes. (n=2 for Cre_Oil, n=3 for IRF3-2D,Cre_Oil). B Gene ontology analysis (biological process) and Reactome analysis of the upregulated genes in A shows activation of pathways related to leukocyte migration and chemotaxis (yellow arrows), activation of viral response (black arrows antigen presentation (red arrow), immune response pathways (light blue arrow), NOD like receptor signaling pathway (Green arrow) and ER-phagosome pathway (purple arrow).

Supplementary Material 6. Table 1.

Acknowledgements
We would like to thank NIH and NIAAA grants for funding and support. Figures-schematics were created using BioRender.com. We would like to thank Dr. Evan Rosen for generous gift of IRF3-2D (C57BL/6-Gt(ROSA)26Sortm4(CAG-Irf3*S388D*S390D)Evdr/J-036261) mice.

Author contributions
R.J. and G.S. conceptualized and wrote the manuscript. R.J., V.B., M.O.-R., Y.Z., A.Z. performed experiments and analysed data. G.M., S.B. performed and reviewed image analysis. S.G.-M., J.G.-S. performed and reviewed analysis of the RNAseq data. All authors contributed to editing of the manuscript.

Funding
This study was supported by NIH grant-R01AG072899 and NIAAA grant-5R01AA017729.

Data availability
The datasets used and/or analysed during the current study are available from the corresponding author on reasonable request.

Declarations

Ethics approval and consent to participate
All the breedings, experiments and euthanasia were conducted as per the institutional ethics and IACUC protocol 030-2022.

Competing interests
G.S. was the editor-in-Chief of Hepatology Communication., consults for Cyta Therapeutics, Durect, Evive, Merck, Novartis, Pandion Therapeutics, Pfizer, Surrozen and Terra Firma, received royalties from UptoDate and Springer and also holds equity in Glympse Bio, Zomagen and Satellite Bio.

Received: 11 March 2024 Accepted: 12 August 2024
Published online: 30 August 2024

References

1. Platanias LC. Mechanisms of type-I- and type-II-interferon-mediated signalling. Nat Rev Immunol. 2005;5:375–86.
2. McNab F, Mayer-Barber K, Sher A, Wack A, O'Garra A. Type I interferons in infectious disease. Nat Rev Immunol. 2015;15:87–103.
3. Jin M, Xu R, Wang L, Alam MM, Ma Z, Zhu S, Martini AC, Jadali A, Bernabucci M, Xie P, Kwan KY, Pang ZP, Head E, Liu Y, Hart RP, Jiang P. Type-I-interferon signaling drives microglial dysfunction and senescence in human iPSC models of down syndrome and Alzheimer's disease. Cell Stem Cell. 2022;29:1135-1153.e8.
4. Roy ER, Wang B, Wan YW, Chiu G, Cole A, Yin Z, Propson NE, Xu Y, Jankowsky JL, Liu Z, Lee VM, Trojanowski JQ, Ginsberg SD, Butovsky O, Zheng H, Cao W. Type I interferon response drives neuroinflammation and synapse loss in Alzheimer disease. J Clin Invest. 2020;130:1912–30.
5. Roy ER, Chiu G, Li S, Propson NE, Kanchi R, Wang B, Coarfa C, Zheng H, Cao W. Concerted type I interferon signaling in microglia and neural cells promotes memory impairment associated with amyloid β plaques. Immunity. 2022;55:879-894.e6.
6. Barrett JP, Knoblach SM, Bhattacharya S, Gordish-Dressman H, Stoica BA, Loane DJ. Traumatic brain injury induces cGAS activation and type I interferon signaling in aged mice. Front Immunol. 2021;12: 710608.
7. Abdullah A, Zhang M, Frugier T, Bedoui S, Taylor JM, Crack PJ. STING-mediated type-I interferons contribute to the neuroinflammatory process and detrimental effects following traumatic brain injury. J Neuroinflammation. 2018;15:323.
8. Kong L, Li W, Chang E, Wang W, Shen N, Xu X, Wang X, Zhang Y, Sun W, Hu W, Xu P, Liu X. mtDNA-STING axis mediates microglial polarization via IRF3/NF-κB signaling after ischemic stroke. Front Immunol. 2022;13: 860977.
9. Ben-Yehuda H, Matcovitch-Natan O, Kertser A, Spinrad A, Prinz M, Amit I, Schwartz M. Maternal Type-I interferon signaling adversely affects the microglia and the behavior of the offspring accompanied by increased sensitivity to stress. Mol Psychiatr. 2020;25:1050–67.
10. Li J, Pang Y, Du Y, Xia L, Chen M, Fan Y, Dong Z. Lack of interferon regulatory factor 3 leads to anxiety/depression-like behaviors through disrupting the balance of neuronal excitation and inhibition in mice. Genes Dis. 2023;10:1062–74.
11. Suzzi S, Tsitsou-Kampeli A, Schwartz M. The type I interferon antiviral response in the choroid plexus and the cognitive risk in COVID-19. Nat Immunol. 2023;24:220–4.
12. Crow YJ, Stetson DB. The type I interferonopathies: 10 years on. Nat Rev Immunol. 2022;22:471–83.
13. Salih DA, Bayram S, Guelfi S, Reynolds RH, Shoai M, Ryten M, Brenton JW, Zhang D, Matarin M, Botia JA, Shah R, Brookes KJ, Guetta-Baranes T, Morgan K, Bellou E, Cummings DM, Escott-Price V, Hardy J. Genetic variability in response to amyloid beta deposition influences Alzheimer's disease risk. Brain Commun. 2019;1:fcz022.
14. Sala Frigerio C, Wolfs L, Fattorelli N, Thrupp N, Voytyuk I, Schmidt I, Mancuso R, Chen WT, Woodbury ME, Srivastava G, Möller T, Hudry E, Das S, Saido T, Karran E, Hyman B, Perry VH, Fiers M, De Strooper B. The major risk factors for Alzheimer's disease: age, sex, and genes modulate the microglia response to Aβ plaques. Cell Rep. 2019;27:1293-1306.e6.
15. Olah M, Menon V, Habib N, Taga MF, Ma Y, Yung CJ, Cimpean M, Khairallah A, Coronas-Samano G, Sankowski R, Grün D, Kroshilina AA, Dionne D, Sarkis RA, Cosgrove GR, Helgager J, Golden JA, Pennell PB, Prinz M, Vonsattel JPG, Teich AF, Schneider JA, Bennett DA, Regev A, Elyaman W, Bradshaw EM, De Jager PL. Single cell RNA sequencing of human microglia uncovers a subset associated with Alzheimer's disease. Nat Commun. 2020;11:6129.
16. Hammond TR, Dufort C, Dissing-Olesen L, Giera S, Young A, Wysoker A, Walker AJ, Gergits F, Segel M, Nemesh J, Marsh SE, Saunders A, Macosko E, Ginhoux F, Chen J, Franklin RJM, Piao X, McCarroll SA, Stevens B. Single-cell RNA sequencing of microglia throughout the mouse lifespan and in the injured brain reveals complex cell-state changes. Immunity. 2019;50:253-271.e6.
17. Hasel P, Rose IVL, Sadick JS, Kim RD, Liddelow SA. Neuroinflammatory astrocyte subtypes in the mouse brain. Nat Neurosci. 2021;24:1475–87.
18. Kaya T, Mattugini N, Liu L, Ji H, Cantuti-Castelvetri L, Wu J, Schifferer M, Groh J, Martini R, Besson-Girard S, Kaji S, Liesz A, Gokce O, Simons M. CD8(+) T cells induce interferon-responsive oligodendrocytes and microglia in white matter aging. Nat Neurosci. 2022;25:1446–57.

19. Honda K, Takaoka A, Taniguchi T. Type I interferon [corrected] gene induction by the interferon regulatory factor family of transcription factors. Immunity. 2006;25:349–60.
20. Sakaguchi S, Negishi H, Asagiri M, Nakajima C, Mizutani T, Takaoka A, Honda K, Taniguchi T. Essential role of IRF-3 in lipopolysaccharide-induced interferon-beta gene expression and endotoxin shock. Biochem Biophys Res Commun. 2003;306:860–6.
21. Fitzgerald KA, Rowe DC, Barnes BJ, Caffrey DR, Visintin A, Latz E, Monks B, Pitha PM, Golenbock DT. LPS-TLR4 signaling to IRF-3/7 and NF-kappaB involves the toll adapters TRAM and TRIF. J Exp Med. 2003;198:1043–55.
22. Patel SJ, Liu N, Piaker S, Gulko A, Andrade ML, Heyward FD, Sermersheim T, Edinger N, Srinivasan H, Emont MP, Westcott GP, Luther J, Chung RT, Yan S, Kumari M, Thomas R, Deleye Y, Tchernof A, White PJ, Baselli GA, Meroni M, De Jesus DF, Ahmad R, Kulkarni RN, Valenti L, Tsai L, Rosen ED. Hepatic IRF3 fuels dysglycemia in obesity through direct regulation of Ppp2r1b. Sci Transl Med. 2022;14:eabh3831.
23. Yan S, Kumari M, Xiao H, Jacobs C, Kochumon S, Jedrychowski M, Chouchani E, Ahmad R, Rosen ED. IRF3 reduces adipose thermogenesis via ISG15-mediated reprogramming of glycolysis. J Clin Invest. 2021. https://doi.org/10.1172/JCI144888.
24. Zhuang Y, Ortega-Ribera M, Thevkar Nagesh P, Joshi R, Huang H, Wang Y, Zivny A, Mehta J, Parikh SM, Szabo G. Bile acid-induced IRF3 phosphorylation mediates cell death, inflammatory responses and fibrosis in cholestasis-induced liver and kidney injury via regulation of ZBP1. Hepatology. 2023;79(4):752–67. https://doi.org/10.1097/HEP.0000000000000611.
25. Yanai H, Chiba S, Hangai S, Kometani K, Inoue A, Kimura Y, Abe T, Kiyonari H, Nishio J, Taguchi-Atarashi N, Mizushima Y, Negishi H, Grosschedl R, Taniguchi T. Revisiting the role of IRF3 in inflammation and immunity by conditional and specifically targeted gene ablation in mice. Proc Natl Acad Sci U S A. 2018;115:5253–8.
26. Salvador AF, de Lima KA, Kipnis J. Neuromodulation by the immune system: a focus on cytokines. Nat Rev Immunol. 2021;21:526–41.
27. Dantzer R. Cytokine sickness behavior and depression. Immunol Allerg Clin N Am. 2009;29(2):247–64. https://doi.org/10.1016/j.iac.2009.02.002
28. Czerkies M, Korwek Z, Prus W, Kochańczyk M, Jaruszewicz-Błońska J, Tudelska K, Błoński S, Kimmel M, Brasier AR, Lipniacki T. Cell fate in antiviral response arises in the crosstalk of IRF NF-κB and JAK/STAT pathways. Nat Commun. 2018;9:493.
29. Mandrekar P, Szabo G. Signalling pathways in alcohol-induced liver inflammation. J Hepatol. 2009;50:1258–66.
30. Zhang Y, Chen K, Sloan SA, Bennett ML, Scholze AR, O'Keeffe S, Phatnani HP, Guarnieri P, Caneda C, Ruderisch N, Deng S, Liddelow SA, Zhang C, Daneman R, Maniatis T, Barres BA, Wu JQ. An RNA-sequencing transcriptome and splicing database of glia, neurons, and vascular cells of the cerebral cortex. J Neurosci. 2014;34:11929–47.
31. Ma W, Oliveira-Nunes MC, Xu K, Kossenkov A, Reiner BC, Crist RC, Hayden J, Chen Q. Type I interferon response in astrocytes promotes brain metastasis by enhancing monocytic myeloid cell recruitment. Nat Commun. 2023;14:2632.
32. Zhu W, Cao FS, Feng J, Chen HW, Wan JR, Lu Q, Wang J. NLRP3 inflammasome activation contributes to long-term behavioral alterations in mice injected with lipopolysaccharide. Neuroscience. 2017;343:77–84.
33. Faust TE, Feinberg PA, O'Connor C, Kawaguchi R, Chan A, Strasburger H, Frosch M, Boyle MA, Masuda T, Amann L, Knobeloch KP, Prinz M, Schaefer A, Schafer DP. A comparative analysis of microglial inducible Cre lines. Cell Rep. 2023;42: 113031.
34. Krasemann S, Madore C, Cialic R, Baufeld C, Calcagno N, El Fatimy R, Beckers L, O'Loughlin E, Xu Y, Fanek Z, Greco DJ, Smith ST, Tweet G, Humulock Z, Zrzavy T, Conde-Sanroman P, Gacias M, Weng Z, Chen H, Tjon E, Mazaheri F, Hartmann K, Madi A, Ulrich JD, Glatzel M, Worthmann A, Heeren J, Budnik B, Lemere C, Ikezu T, Heppner FL, Litvak V, Holtzman DM, Lassmann H, Weiner HL, Ochando J, Haass C, Butovsky O. The TREM2-APOE pathway drives the transcriptional phenotype of dysfunctional microglia in neurodegenerative diseases. Immunity. 2017;47(566–581): e9.
35. Deczkowska A, Keren-Shaul H, Weiner A, Colonna M, Schwartz M, Amit I. Disease-associated microglia: a universal immune sensor of neurodegeneration. Cell. 2018;173:1073–81.
36. Keren-Shaul H, Spinrad A, Weiner A, Matcovitch-Natan O, Dvir-Szternfeld R, Ulland TK, David E, Baruch K, Lara-Astaiso D, Toth B, Itzkovitz S, Colonna M, Schwartz M, Amit I. A unique microglia type associated with restricting development of Alzheimer's disease. Cell. 2017;169(1276–1290): e17.
37. Friedman BA, Srinivasan K, Ayalon G, Meilandt WJ, Lin H, Huntley MA, Cao Y, Lee SH, Haddick PCG, Ngu H, Modrusan Z, Larson JL, Kaminker JS, van der Brug MP, Hansen DV. Diverse brain myeloid expression profiles reveal distinct microglial activation states and aspects of Alzheimer's disease not evident in mouse models. Cell Rep. 2018;22:832–47.
38. Kuriakose T, Kanneganti TD. ZBP1: innate sensor regulating cell death and inflammation. Trend Immunol. 2018;39:123–34.
39. Muendlein HI, Connolly WM, Magri Z, Jetton D, Smirnova I, Degterev A, Balachandran S, Poltorak A. ZBP1 promotes inflammatory responses downstream of TLR3/TLR4 via timely delivery of RIPK1 to TRIF. Proc Natl Acad Sci U S A. 2022;119: e2113872119.
40. Petrasek J, Iracheta-Vellve A, Csak T, Satishchandran A, Kodys K, Kurt-Jones EA, Fitzgerald KA, Szabo G. STING-IRF3 pathway links endoplasmic reticulum stress with hepatocyte apoptosis in early alcoholic liver disease. Proc Natl Acad Sci U S A. 2013;110:16544–9.
41. Andersen LL, Mørk N, Reinert LS, Kofod-Olsen E, Narita R, Jørgensen SE, Skipper KA, Höning K, Gad HH, Østergaard L, Ørntoft TF, Hornung V, Paludan SR, Mikkelsen JG, Fujita T, Christiansen M, Hartmann R, Mogensen TH. Functional IRF3 deficiency in a patient with herpes simplex encephalitis. J Exp Med. 2015;212:1371–9.
42. Canivet C, Rhéaume C, Lebel M, Piret J, Gosselin J, Boivin G. Both IRF3 and especially IRF7 play a key role to orchestrate an effective cerebral inflammatory response in a mouse model of herpes simplex virus encephalitis. J Neurovirol. 2018;24:761–8.
43. Schultz KLW, Troisi EM, Baxter VK, Glowinski R, Griffin DE. Interferon regulatory factors 3 and 7 have distinct roles in the pathogenesis of alphavirus encephalomyelitis. J Gen Virol. 2019;100:46–62.
44. Motwani M, Pesiridis S, Fitzgerald KA. DNA sensing by the cGAS-STING pathway in health and disease. Nat Rev Genet. 2019;20:657–74.
45. Hopfner KP, Hornung V. Molecular mechanisms and cellular functions of cGAS-STING signalling. Nat Rev Mol Cell Biol. 2020;21:501–21.
46. Hou Y, Wei Y, Lautrup S, Yang B, Wang Y, Cordonnier S, Mattson MP, Croteau DL, Bohr VA. NAD(+) supplementation reduces neuroinflammation and cell senescence in a transgenic mouse model of Alzheimer's disease via cGAS-STING. Proc Natl Acad Sci U S A. 2021;118(37):e2011226118. https://doi.org/10.1073/pnas.2011226118.
47. Paul BD, Snyder SH, Bohr VA. Signaling by cGAS-STING in neurodegeneration, neuroinflammation, and aging. Trend Neurosci. 2021;44:83–96.
48. Calvo-Rodriguez M, García-Rodríguez C, Villalobos C, Núñez L. Role of toll like receptor 4 in Alzheimer's disease. Front Immunol. 2020;11:1588.
49. Heidari A, Yazdanpanah N, Rezaei N. The role of toll-like receptors and neuroinflammation in Parkinson's disease. J Neuroinflammation. 2022;19:135.
50. Zheng C, Chen J, Chu F, Zhu J, Jin T. Inflammatory role of TLR-MyD88 signaling in multiple sclerosis. Front Mol Neurosci. 2019;12:314.
51. Lee JY, Lee JD, Phipps S, Noakes PG, Woodruff TM. Absence of toll-like receptor 4 (TLR4) extends survival in the hSOD1 G93A mouse model of amyotrophic lateral sclerosis. J Neuroinflammation. 2015;12:90.
52. Kawasaki T, Kawai T. Toll-like receptor signaling pathways. Front Immunol. 2014;5:461.
53. Kim S, Kim SY, Pribis JP, Lotze M, Mollen KP, Shapiro R, Loughran P, Scott MJ, Billiar TR. Signaling of high mobility group box 1 (HMGB1) through toll-like receptor 4 in macrophages requires CD14. Mol Med. 2013;19:88–98.
54. Peek V, Harden LM, Damm J, Aslani F, Leisengang S, Roth J, Gerstberger R, Meurer M, von Köckritz-Blickwede M, Schulz S, Spengler B, Rummel C. LPS primes brain responsiveness to high mobility group box-1 protein. Pharmaceuticals. 2021;14(6):558. https://doi.org/10.3390/ph14060558.
55. Hritz I, Mandrekar P, Velayudham A, Catalano D, Dolganiuc A, Kodys K, Kurt-Jones E, Szabo G. The critical role of toll-like receptor (TLR) 4 in alcoholic liver disease is independent of the common TLR adapter MyD88. Hepatology. 2008;48:1224–31.
56. Dantzer R. Cytokine, sickness behavior, and depression. Neurol Clin. 2006;24:441–60.
57. Morrison DC, Kline LF. Activation of the classical and properdin pathways of complement by bacterial lipopolysaccharides (LPS). J Immunol. 1977;118:362–8.
58. Käufer C, Chhatbar C, Bröer S, Waltl I, Ghita L, Gerhauser I, Kalinke U, Löscher W. Chemokine receptors CCR2 and CX3CR1 regulate viral

encephalitis-induced hippocampal damage but not seizures. Proc Natl Acad Sci U S A. 2018;115:E8929-e8938.
59. Heneka MT, Kummer MP, Stutz A, Delekate A, Schwartz S, Vieira-Saecker A, Griep A, Axt D, Remus A, Tzeng TC, Gelpi E, Halle A, Korte M, Latz E, Golenbock DT. NLRP3 is activated in Alzheimer's disease and contributes to pathology in APP/PS1 mice. Nature. 2013;493:674–8.
60. Zhou K, Shi L, Wang Y, Chen S, Zhang J. Recent advances of the NLRP3 inflammasome in central nervous system disorders. J Immunol Res. 2016;2016:9238290.
61. Li N, Zhou H, Wu H, Wu Q, Duan M, Deng W, Tang Q. STING-IRF3 contributes to lipopolysaccharide-induced cardiac dysfunction, inflammation, apoptosis and pyroptosis by activating NLRP3. Redox Biol. 2019;24: 101215.
62. Baxter PS, Dando O, Emelianova K, He X, McKay S, Hardingham GE, Qiu J. Microglial identity and inflammatory responses are controlled by the combined effects of neurons and astrocytes. Cell Rep. 2021;34: 108882.
63. Doyle S, Vaidya S, O'Connell R, Dadgostar H, Dempsey P, Wu T, Rao G, Sun R, Haberland M, Modlin R, Cheng G. IRF3 mediates a TLR3/TLR4-specific antiviral gene program. Immunity. 2002;17:251–63.
64. Kim ID, Ha BJ. Paeoniflorin protects RAW 264.7 macrophages from LPS-induced cytotoxicity and genotoxicity. Toxicol In Vitro. 2009;23:1014–9.
65. Samivel R, Subramanian U, Ali Khan A, Kirat O, Masmali A, Almubrad T, Akhtar S. Lipopolysaccharide enhances genotoxicity by activating GADD45G and NF-κB in human corneal epithelial cells. Oxid Med Cell Longev. 2022;2022:4328116.
66. Lee S, Devanney NA, Golden LR, Smith CT, Schwartz JL, Walsh AE, Clarke HA, Goulding DS, Allenger EJ, Morillo-Segovia G, Friday CM, Gorman AA, Hawkinson TR, MacLean SM, Williams HC, Sun RC, Morganti JM, Johnson LA. APOE modulates microglial immunometabolism in response to age, amyloid pathology, and inflammatory challenge. Cell Rep. 2023;42: 112196.
67. Ulrich JD, Ulland TK, Mahan TE, Nyström S, Nilsson KP, Song WM, Zhou Y, Reinartz M, Choi S, Jiang H, Stewart FR, Anderson E, Wang Y, Colonna M, Holtzman DM. ApoE facilitates the microglial response to amyloid plaque pathology. J Exp Med. 2018;215:1047–58.
68. Shi Y, Manis M, Long J, Wang K, Sullivan PM, Remolina Serrano J, Hoyle R, Holtzman DM. Microglia drive APOE-dependent neurodegeneration in a tauopathy mouse model. J Exp Med. 2019;216:2546–61.
69. Sahasrabuddhe V, Ghosh HS. Cx3Cr1-Cre induction leads to microglial activation and IFN-1 signaling caused by DNA damage in early postnatal brain. Cell Rep. 2022;38: 110252.
70. Barrett JP, Henry RJ, Shirey KA, Doran SJ, Makarevich OD, Ritzel RM, Meadows VA, Vogel SN, Faden AI, Stoica BA, Loane DJ. Interferon-β plays a detrimental role in experimental traumatic brain injury by enhancing neuroinflammation that drives chronic neurodegeneration. J Neurosci. 2020;40:2357–70.
71. Tripathi A, Whitehead C, Surrao K, Pillai A, Madeshiya A, Li Y, Khodadadi H, Ahmed AO, Turecki G, Baban B, Pillai A. Type 1 interferon mediates chronic stress-induced neuroinflammation and behavioral deficits via complement component 3-dependent pathway. Mol Psychiatr. 2021;26:3043–59.
72. Penner IK, Stemper B, Calabrese P, Freedman MS, Polman CH, Edan G, Hartung HP, Miller DH, Montalbán X, Barkhof F, Pleimes D, Lanius V, Pohl C, Kappos L, Sandbrink R. Effects of interferon beta-1b on cognitive performance in patients with a first event suggestive of multiple sclerosis. Mult Scler. 2012;18:1466–71.
73. Lacy M, Hauser M, Pliskin N, Assuras S, Valentine MO, Reder A. The effects of long-term interferon-beta-1b treatment on cognitive functioning in multiple sclerosis: a 16 year longitudinal study. Mult Scler. 2013;19:1765–72.
74. De S, Wirthensohn DC, Flagmeier P, Hughes C, Aprile FA, Ruggeri FS, Whiten DR, Emin D, Xia Z, Varela JA, Sormanni P, Kundel F, Knowles TPJ, Dobson CM, Bryant C, Vendruscolo M, Klenerman D. Different soluble aggregates of Aβ42 can give rise to cellular toxicity through different mechanisms. Nat Commun. 2019;10:1541.
75. Jin M, Shiwaku H, Tanaka H, Obita T, Ohuchi S, Yoshioka Y, Jin X, Kondo K, Fujita K, Homma H, Nakajima K, Mizuguchi M, Okazawa H. Tau activates microglia via the PQBP1-cGAS-STING pathway to promote brain inflammation. Nat Commun. 2021;12:6565.
76. Pampuscenko K, Morkuniene R, Krasauskas L, Smirnovas V, Brown GC, Borutaite V. Extracellular tau stimulates phagocytosis of living neurons by activated microglia via Toll-like 4 receptor-NLRP3 inflammasome-caspase-1 signalling axis. Sci Rep. 2023;13:10813.
77. Peng R, Wang CK, Wang-Kan X, Idorn M, Kjaer M, Zhou FY, Fiil BK, Timmermann F, Orozco SL, McCarthy J, Leung CS, Lu X, Bagola K, Rehwinkel J, Oberst A, Maelfait J, Paludan SR, Gyrd-Hansen M. Human ZBP1 induces cell death-independent inflammatory signaling via RIPK3 and RIPK1. EMBO Rep. 2022;23: e55839.
78. Guo H, Chen R, Li P, Yang Q, He Y. ZBP1 mediates the progression of Alzheimer's disease via pyroptosis by regulating IRF3. Mol Cell Biochem. 2023. https://doi.org/10.1007/s11010-023-04702-6.
79. Baik SH, Kang S, Lee W, Choi H, Chung S, Kim JI, Mook-Jung I. A breakdown in metabolic reprogramming causes microglia dysfunction in Alzheimer's disease. Cell Metab. 2019;30:493–507.e6.
80. Wang RG, Kaul M, Zhang DX. Interferon-stimulated gene 15 as a general marker for acute and chronic neuronal injuries. Sheng Li Xue Bao. 2012;64:577–83.
81. Guo X, Wiley CA, Steinman RA, Sheng Y, Ji B, Wang J, Zhang L, Wang T, Zenatai M, Billiar TR, Wang Q. Aicardi-Goutières syndrome-associated mutation at ADAR1 gene locus activates innate immune response in mouse brain. J Neuroinflammation. 2021;18:169.
82. De Masi R, Orlando S, Bagordo F, Grassi T. IFP35 is a relevant factor in innate immunity, multiple sclerosis, and other chronic inflammatory diseases: a review. Biology (Basel). 2021. https://doi.org/10.3390/biology10121325.
83. Vitner EB, Farfel-Becker T, Ferreira NS, Leshkowitz D, Sharma P, Lang KS, Futerman AH. Induction of the type I interferon response in neurological forms of Gaucher disease. J Neuroinflammation. 2016;13:104.
84. Lang R, Li H, Luo X, Liu C, Zhang Y, Guo S, Xu J, Bao C, Dong W, Yu Y. Expression and mechanisms of interferon-stimulated genes in viral infection of the central nervous system (CNS) and neurological diseases. Front Immunol. 2022;13:1008072.
85. Fourgeaud L, Través PG, Tufail Y, Leal-Bailey H, Lew ED, Burrola PG, Callaway P, Zagórska A, Rothlin CV, Nimmerjahn A, Lemke G. TAM receptors regulate multiple features of microglial physiology. Nature. 2016;532:240–4.
86. Wu T, Dejanovic B, Gandham VD, Gogineni A, Edmonds R, Schauer S, Srinivasan K, Huntley MA, Wang Y, Wang TM, Hedehus M, Barck KH, Stark M, Ngu H, Foreman O, Meilandt WJ, Elstrott J, Chang MC, Hansen DV, Carano RAD, Sheng M, Hanson JE. Complement C3 is activated in human AD brain and is required for neurodegeneration in mouse models of amyloidosis and tauopathy. Cell Rep. 2019;28:2111-2123.e6.
87. Werneburg S, Jung J, Kunjamma RB, Ha SK, Luciano NJ, Willis CM, Gao G, Biscola NP, Havton LA, Crocker SJ, Popko B, Reich DS, Schafer DP. Targeted complement inhibition at synapses prevents microglial synaptic engulfment and synapse loss in demyelinating disease. Immunity. 2020;52:167-182.e7.
88. Nakajima A, Nishimura K, Nakaima Y, Oh T, Noguchi S, Taniguchi T, Tamura T. Cell type-dependent proapoptotic role of Bcl2L12 revealed by a mutation concomitant with the disruption of the juxtaposed Irf3 gene. Proc Natl Acad Sci U S A. 2009;106:12448–52.
89. Marsh SE, Walker AJ, Kamath T, Dissing-Olesen L, Hammond TR, de Soysa TY, Young AMH, Murphy S, Abdulraouf A, Nadaf N, Dufort C, Walker AC, Lucca LE, Kozareva V, Vanderburg C, Hong S, Bulstrode H, Hutchinson PJ, Gaffney DJ, Hafler DA, Franklin RJM, Macosko EZ, Stevens B. Dissection of artifactual and confounding glial signatures by single-cell sequencing of mouse and human brain. Nat Neurosci. 2022;25:306–16.
90. Friker LL, Scheiblich H, Hochheiser IV, Brinkschulte R, Riedel D, Latz E, Geyer M, Heneka MT. β-amyloid clustering around ASC fibrils boosts its toxicity in microglia. Cell Rep. 2020;30:3743-3754.e6.

Publisher's Note